

Inhibition of Sphingosine-1-Phosphate Lyase for the Treatment of Autoimmune Disorders

Jeffrey T. Bagdanoff,^{*,†} Michael S. Donoviel,[‡] Amr Nouraldeen,[‡] James Tarver,[†] Qinghong Fu,[†] Marianne Carlsen,[†] Theodore C. Jessop,[†] Haiming Zhang,[†] Jill Hazelwood,[‡] Huy Nguyen,[†] Simon D. P. Baugh,[†] Michael Gardyan,[†] Kristen M. Terranova,[†] Joseph Barbosa,[†] Jack Yan,[†] Mark Bednarz,[†] Suman Layek,[†] Lawrence F. Courtney,[†] Jerry Taylor,[†] Ann Marie Digeorge-Foushee,[‡] Suma Gopinathan,[‡] Debra Bruce,[‡] Traci Smith,[‡] Liam Moran,[‡] Emily O'Neill,[‡] Jeff Kramer,[‡] Zhong Lai,[†] S. David Kimball,[†] Qingyun Liu,[‡] Weimei Sun,[‡] Sean Yu,[‡] Jonathan Swaffield,[‡] Alan Wilson,[‡] Alan Main,[†] Kenneth G. Carson,[†] Tamas Oravecz,[‡] and David J. Augeri^{*,†}

Lexicon Pharmaceuticals, 350 Carter Road, Princeton, New Jersey, 08540, Lexicon Pharmaceuticals, 8800 Technology Forest Place, The Woodlands, Texas 77381

Received March 4, 2009

During nearly a decade of research dedicated to the study of sphingosine signaling pathways, we identified sphingosine-1-phosphate lyase (S1PL) as a drug target for the treatment of autoimmune disorders. S1PL catalyzes the irreversible decomposition of sphingosine-1-phosphate (S1P) by a retro-aldol fragmentation that yields hexadecanaldehyde and phosphoethanolamine. Genetic models demonstrated that mice expressing reduced S1PL activity had decreased numbers of circulating lymphocytes due to altered lymphocyte trafficking, which prevented disease development in multiple models of autoimmune disease. Mechanistic studies of lymphoid tissue following oral administration of 2-acetyl-4(5)-(1*R*),2(*S*),3(*R*),4-tetrahydroxybutyl)-imidazole (THI) **3** showed a clear relationship between reduced lyase activity, elevated S1P levels, and lower levels of circulating lymphocytes. Our internal medicinal chemistry efforts discovered potent analogues of **3** bearing heterocycles as chemical equivalents of the pendant carbonyl present in the parent structure. Reduction of S1PL activity by oral administration of these analogues recapitulated the phenotype of mice with genetically reduced S1PL expression.

Introduction

Sphingolipids represent a wide array of naturally occurring, amphiphilic modulators of eukaryotic cell-signaling. Containing polar head groups, multiple hydroxyls, a free amino group, and lengthy lipid chains, specific members of this family are key mediators of intra- and extracellular signaling.¹ Sphingosine-1-phosphate (S1P^a)² (Figure 1), enzymatically derived from ceramide, is a key signaling lipid. S1P is present in all mammalian cells and can serve as a secondary messenger in the signal transduction pathways that regulate the vascular and immune systems, cell differentiation, and apoptosis.³ It is also released into the extracellular milieu by a variety of cell types, making it one of the most abundant biologically active lysophospholipids in circulation.⁴ S1P functions as an extracellular ligand for G-protein-coupled receptors (GPCRs) that regulate T- and B-cell trafficking.⁵ Five S1P-binding GPCRs (S1P1–S1P5) have been identified thus far and are expressed in many tissues.⁶ Agonism of S1P1 results in lymphopenia, while agonism of S1P3 is associated with bradycardia.

Investigation into natural products structurally related to S1P, such as myriocin,⁷ implicated control of specific key sphingolipid signaling events as a potential treatment for autoimmune diseases. In vivo studies with myriocin demonstrated the

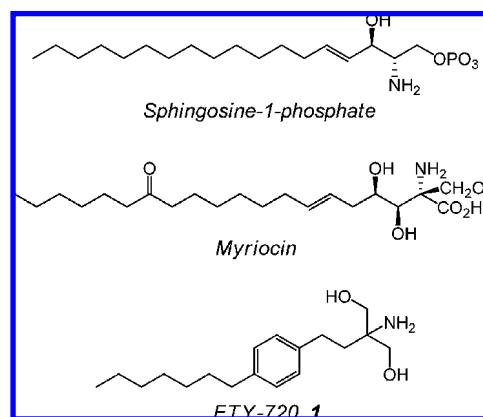


Figure 1. Structure of sphingosine-1-phosphate, myriocin, and **1**.

therapeutic potential of modulating sphingolipid signaling with sphingolipid-like analogues⁸ and preceded the development of FTY-720 **1**,⁹ which is structurally homologous to both myriocin and sphingosine. A functional consequence of S1P or **1** binding to S1P1 is receptor internalization, which eventually leads to inhibition of lymphocyte egress from secondary lymphoid tissues, resulting in peripheral lymphopenia. These discoveries led to a closer examination of the importance of S1P gradients and sphingosine-based signaling in immune regulation.

Endogenous levels of S1P can be influenced by modulating the activity of the enzymes involved in its synthesis and degradation. The relationship between S1P and its receptors, and the array and function of sphingolipid enzymes, has been recently reviewed.¹⁰ Sphingosine is produced by enzymatic degradation of ceramide.¹¹ Sphingosine kinase 1 (SK1) and sphingosine kinase 2 (SK2) phosphorylate sphingosine to S1P,¹² while S1P phosphatase catalyzes the reverse reaction.¹³ Alternatively, intracellular S1P concentrations are attenuated by S1P

* To whom correspondence should be addressed. For D.A.: phone, (609) 466-5526; fax, (609) 466-6079; E-mail: daugeri@lexpharma.com. For J.B.: phone, (609) 466-5583; fax, (609) 466-6079; E-mail, jbagdanoff@lexpharma.com.

[†] Lexicon Pharmaceuticals, Princeton, NJ.

[‡] Lexicon Pharmaceuticals, The Woodlands, TX.

^a Abbreviations: THI, 2-acetyl-4(5)-(1*R*),2(*S*),3(*R*),4-tetrahydroxybutyl)-imidazole; S1P, sphingosine-1-phosphate; S1PL, sphingosine-1-phosphate lyase; KO, knockout; S1P1, sphingosine-1-phosphate receptor 1; SK1, sphingosine kinase 1; SK2, sphingosine kinase 2; GPCR, G-protein-coupled receptor; CBC, complete blood count; SAR, structure–activity relationship; ADME, absorption, distribution, metabolism, excretion; DOP, deoxyppyridoxine.

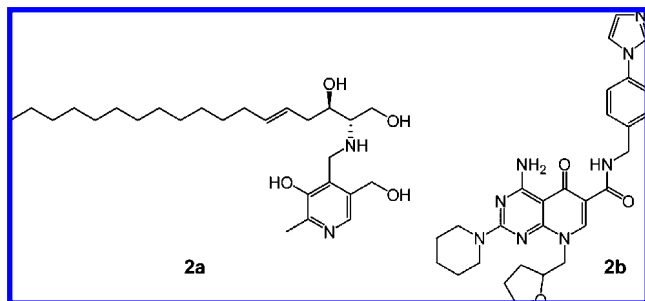


Figure 2. Structure of S1P transition state analogue inhibitor **2a**, oxopyridylpyrimidine **2b**.

lyase (S1PL), which, aided by the cofactor pyridoxal phosphate, catalyzes the irreversible retro-Aldol fragmentation of S1P to hexadecanal and phosphoethanolamine. Inhibition of S1PL therefore increases endogenous S1P concentrations in lymphoid tissues, providing an alternative approach to modulation of S1P receptors by synthetic ligands.¹⁴ Similar to synthetic S1P receptor agonists, elevated levels of endogenous S1P lead to lower levels of circulating peripheral lymphocytes and mitigates the physiologic outcome of aberrant immune function. Thus, enzymes that mediate the S1P gradient have inspired a new approach for the treatment of autoimmune diseases.

As a part of a high-throughput gene knockout technology platform, we conducted a detailed phenotypic analysis of nearly 5000 independent lines of knockout mice by gene targeting and gene trapping in mouse embryonic stem cells. As a part of this screen, we generated and analyzed several mouse lines deficient in the expression of various enzymes and receptors involved in sphingolipid metabolism and signaling. This work led to the discovery that homozygous S1PL knockout mice exhibit a significant decrease in circulating lymphocytes relative to wild-type cohorts. In mice, only complete knockout of the S1PL gene resulted in traits other than lymphopenia, leading to reduced viability. In the S1PL knockout phenotype, high levels of S1P were observed in the thymus and spleen.¹⁵ In addition to the knockout mice, mouse lines with a wide range of S1PL expression were also established using a genetic knock-in strategy. Mice expressing less than 10% wild type S1PL exhibited lymphopenia without other overt physiological effects. As expected, these mice had an improved outcome in collagen-induced arthritis, indicating that pharmacological inhibition of S1PL represents a novel therapeutic strategy against inflammatory disorders.

Background

We began pursuing S1PL as a potential drug target for the treatment of inflammatory disease through multiple chemical approaches. Initially, de novo design considerations were applied to the S1PL reaction substrate (S1P) and the requisite cofactor (pyridoxal phosphate) to provide precursor **2a** (Figure 2), which we proposed would undergo SK1 or SK2 directed phosphorylation in vivo,¹⁶ generating a functional transition state analogue inhibitor. Compound **2a** was evaluated in vitro, measuring direct enzyme inhibition,¹⁷ and by an in vivo assay, measuring blood lymphocyte levels in whole blood by complete blood count (CBC) four hours following IP administration.¹⁸ Compound **2a** displayed no activity in the biochemical assay, possibly due to inadequate phosphorylation of the two primary alcohols. In addition, **2a** displayed no activity after 100 mg/kg oral administration to mice ($C_{\max} < 1 \mu\text{M}$, $\text{AUC} < 1 \mu\text{M}\cdot\text{h}$).

Oxopyridylpyrimidine **2b** (Figure 2) was identified by HTS. It directly inhibited S1PL ($\text{IC}_{50} = 2.1 \mu\text{M}$) and exhibited cellular

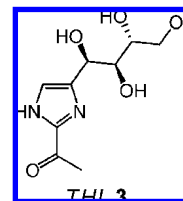
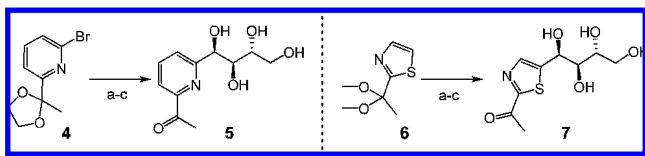


Figure 3. Structure of THI **3**.

activity as well, increasing S1P levels 275% over controls in HepG2 cells. While **2b** registered substantial levels of exposure when dosed to mice at 10 mg/kg ($C_{\max} = 451 \mu\text{M}$, $\text{AUC} = 1872 \mu\text{M}\cdot\text{h}$, $\%F = 100$, $\text{mPPB} > 99\%$), no significant lymphopenia was observed by CBC analysis at either 4 or 18 h following a 100 mg/kg oral dose. The high plasma protein binding may account for the lack of in vivo activity observed. By contrast, in the positive control leg of this experiment, **1** induced substantial lymphopenia at 10 mg/kg, registering greater than 90% reduction in lymphocytes from peripheral circulation. As we were unable to correlate in vitro activity with in vivo pharmacology, we directed further medicinal chemistry efforts toward an alternative chemotype.

2-acetyl-4(5)-(1(R),2(S),3(R),4-tetrahydroxybutyl)-imidazole (THI **3**, Figure 3) is a small molecule present in trace quantities in caramel color III, a popular food colorant produced on an industrial scale by high temperature, high pressure reaction of ammonia with carbohydrates.¹⁹ The immunosuppressive effects of **3** on the immune system have been well documented.²⁰ Interestingly, oral administration of **3** to mice was reported²¹ to result in pharmacology that was strikingly similar to the phenotype that we observed in our mouse line expressing reduced S1PL.¹⁴ Similar pharmacology was observed with deoxypyridoxine (DOP).²⁰ Administration of **3** in drinking water triggered lymphopenia concomitant with decreased S1PL activity and increased S1P levels in lymphoid tissues. Reduced egress of mature CD4+ and CD8+ T cells from lymphoid tissues accounted for lower levels of lymphocytes in peripheral circulation. While no direct enzymatic evidence was offered, the observed pharmacology was attributed to S1PL inhibition. We were intrigued by the striking agreement between the in vivo pharmacology generated by **3** and the phenotype of our mouse lines with reduced S1PL expression.

Our work has been prompted by the recognition that agonism of S1P1 via S1PL inhibition may afford considerable advantages over direct S1P receptor agonism. In particular, synthetic S1P receptor agonists must have selectivity against widely distributed receptor subsets in order to avoid undesired pharmacology. For example, the synthetic S1P receptor agonist **1** is nonselective for S1P1, thus agonizing the S1P3 receptor in heart tissue, causing bradycardia.²² To date, agonists that demonstrate selectivity for S1P1 over S1P3 have yet to advance significantly in human clinical trials. By comparison, because S1PL is expressed primarily in lymphatic tissue, inhibition of S1PL results in the accumulation of endogenous S1P primarily in these tissues. As a consequence of localized S1P concentrations, mice expressing reduced S1PL do not display bradycardia. Advantageously, neutrophil levels are unaffected by S1PL inhibition, unlike the pharmacology observed with S1P agonists. And, unlike with **1**, severe lymphopenia is not observed with lyase inhibition. Our genetic models demonstrate that significant reduction in S1PL expression results only in immunological phenotypes that show significant promise in mitigating the outcome of autoimmune disease. While synthetic S1P1 receptor agonists are currently of high interest in pharmaceutical research

Scheme 1^a

^a Conditions: (a) *n*-BuLi, THF, then 3,4-*O*-isopropylidene-D-erythronolactone, $-78\text{ }^{\circ}\text{C} \rightarrow \text{rt}$; (b) NaBH_4 , *i*-PrOH; (c) aq HCl, acetone.

and development, small molecule inhibitors of S1PL have remained relatively unexplored.

Chemistry

An initial approach toward the construction of analogues of **3** involved installation of the polyhydroxylated side chain onto various heterocyclic cores. Lithiation–halogen exchange of bromopyridine **4** (Scheme 1) preceded addition of 3,4-*O*-isopropylidene-D-erythronolactone, and the intermediate lactol was subsequently reduced and deprotected under acidic conditions to provide pyridine-based tetraol **5**. Thiazole-based tetraol **7**²³ was prepared by the same reaction sequence, beginning with deprotonation of thiazole **6**.

Synthetic methods were also applied directly to **3** to provide other modifications of the core heterocycle. As shown in Scheme 2, *N*-methylated analogue **8** was made by direct alkylation of **3** with methyl iodide under mildly basic conditions. Substitution on the open position of the imidazole ring was accomplished by bis-ketalization of the tetraol side chain of **3** followed by bromination to provide intermediate **9**. Suzuki coupling with a variety of boronic acids followed by deprotection of the tetrahydroxy side chain under acidic conditions furnished analogues **10–12**.

Other chemical approaches were applied to **3** to transform the pendant ketone functionality. Direct reduction of the ketone provided alcohol **13**. Alternatively, condensation with acetylhydrazine provided the acylhydrazone **14**. The ketone was fluorinated to release, after mildly acidic deprotection, difluoride **17**. Other changes at the 2-position of **3** were made following oxidation of the acetyl group. Protection of the tetrahydroxy side chain and imidazole nitrogen followed by haloform reaction provided the protected carboxylic acid **15**, which was converted to amide **16** after peptide coupling and deprotection.

The general synthetic approach used to synthesize **3** (Scheme 3) provided access to multiple analogues. Amadori rearrangement²⁴ of D-glucose with dibenzylamine produced D-fructosamine **18** after hydrogenation of the intermediate *N*-benzyl groups. In the Büchi²⁵ reaction, cyclocondensation between **18** and nitrile **19** constructed the central imidazole ring present in **3** after treatment with acetic acid. The polyhydroxylated side chain stereochemistry derives from the starting sugar. Application of the Büchi cyclocondensation reaction to a variety of nitriles also permitted direct access to a variety of C-2 imidazole analogues. Imidates were generated in situ by reaction of an appropriate nitrile with sodium methoxide and reacted with **18** to afford C-2 substituted imidazoles **20–32** after treatment with acetic acid.

Tandem execution of the Amadori and Büchi reactions also provided a general method to access side chain analogues, deoxygenations, and heteroatom substitutions of **3** (Scheme 4). Amadori rearrangement and Büchi cyclization of D-galactose, L-glucose, D-glucose C-3 methyl ether **35**, and D-glucuronamide

37 provided the C-4 epimer **33**, enantiomer **34**, C-3 methyl ether **36**, and C-6 amide **38**, respectively.

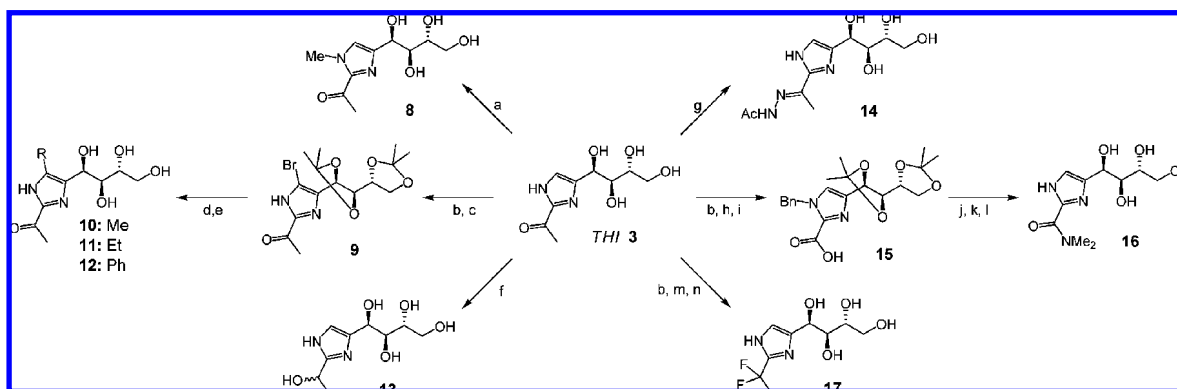
Results and Discussion

Our own internal research, coupled with reports published by other groups,²⁰ strongly supported the notion that the biological activity of **3** was linked to S1PL inhibition. Published results showed that the administration of **3** in drinking water correlated to lymphopenia concomitant with increased concentrations of S1P in lymphoid tissue such as spleen and thymus. While the pharmacology observed following administration of **3** closely resembled the phenotype of mice expressing reduced levels of S1PL, **3** showed no direct inhibition of S1PL when tested in our in vitro assay. However, the role of **3** in reduction of S1PL activity and elevation of S1P was clearly evident in lysates prepared from mouse spleen tissue following oral administration of **3** (100 mg/kg). Tissues were harvested near peak levels of pharmacology (lymphocyte levels by CBC at 18 h, vide infra) and compared directly to vehicle controls. Results showed a significant reduction in lyase activity that was concomitant with a 22-fold increase in S1P levels²⁶ in spleen tissue (Figure 4). This suggested that the established in vivo efficacy was due to a more complex scenario than a simple binary ligand–protein interaction. We considered the possibility that **3** may undergo in vivo processing to an active metabolite. As is the case with **1**, phosphorylation occurs in vivo following oral administration to provide the biologically active ligand.¹⁴ However, detailed analysis of the plasma revealed only the parent compound. Alternatively, S1PL inhibition may be dependent on the formation of a higher-order complex (ternary or higher).²⁷ As a consequence of these findings, we concluded that **3** exerts biological activity by interaction with another ligand, peptide, or protein that then goes on to inhibit S1PL.

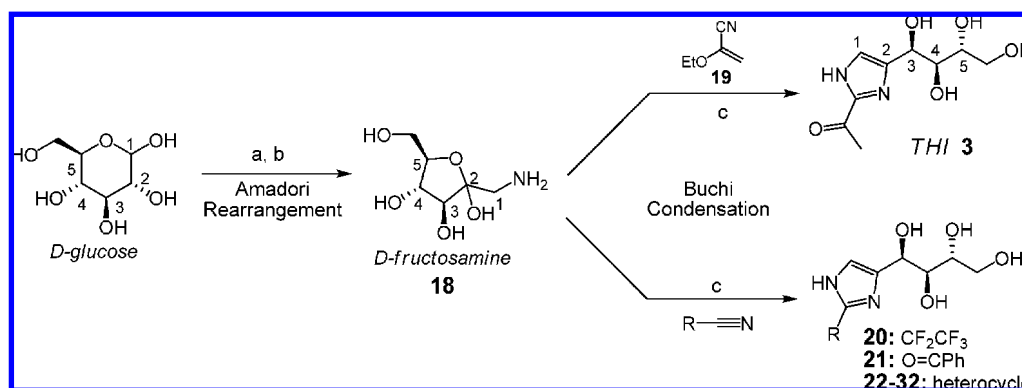
While further elucidation of the mechanistic nuances remained a priority, we were motivated to initiate investigation into the SAR of chemical analogues of **3**. In the absence of an in vitro assay that was predictive of pharmacology, we established an in vivo assay as our primary screen. Our medicinal chemistry efforts focused on structural analogues of **3**, measuring the in vivo activity of our investigational compounds by CBC analysis of lymphocytes in peripheral blood. While in vitro methods are central to the paradigm of modern drug discovery, direct in vivo evaluation of investigational agents is a historically validated approach that accounts for a considerable percentage of marketed drugs.²⁸

Prior to testing analogues, we conducted a detailed pharmacokinetic analysis of **3** to establish a baseline profile (Table 1). From these studies, it was determined that **3** displayed low volume of distribution (0.067 L/kg) and low clearance (2.9 mL/min/kg), providing moderate exposure at a standard oral dose (35.8 $\mu\text{M}\cdot\text{h}$, 10 mg/kg po).

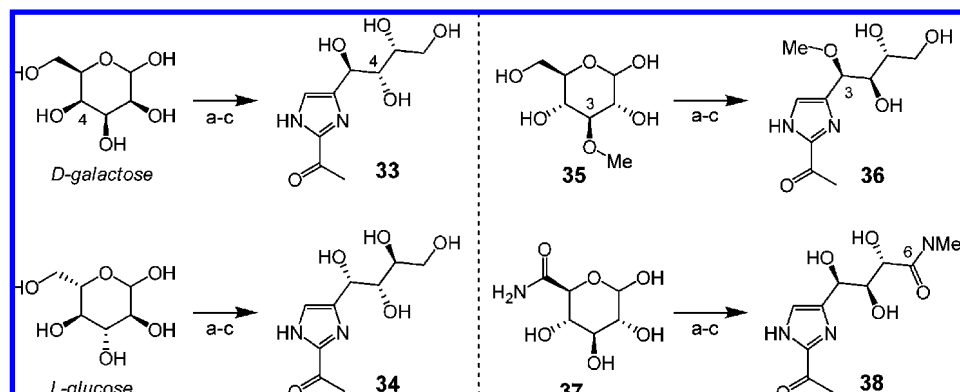
We established the time-dependent relationship between dose and onset of pharmacology. A PK/PD study was conducted whereby **3** was administered at a single 100 mg/kg dose by oral gavage to nine groups of mice ($n = 5$). Each of the nine groups was evaluated for reduction of circulating lymphocytes by CBC analysis at various time points between 0 and 48 h (Figure 5). While circadian rhythm will affect the absolute CBC data taken from mice during the course of a day, this experiment determined that the maximum pharmacodynamic effect (41% reduction) was achieved between 12 and 24 h following a single oral dose. We concluded that 18 h after oral administration constituted a reliable time point for measuring peripheral levels of circulating lymphocytes by CBC analysis.

Scheme 2^a

^a Conditions: (a) K_2CO_3 , MeI, DMF; (b) $(MeO)_2CMe_2$, DCE, *p*-TsOH, 50 °C; (c) Br_2 , DCM:2.0 M aq Na_2CO_3 (1:1), 0 °C; (d) $Pd(dppf)Cl_2$, CsF, DMF; PhMe (1:2), boronic acid, 100 °C; (e) acetone:water:conc HCl (2:2:1); (f) $NaBH_4$, MeOH; (g) $H_2NNH_2 \cdot Ac$, HCl, MeOH; (h) BnBr, K_2CO_3 , DMF; (i) aq NaOCl, NaOH, dioxane; (j) HATU, $Me_2NH \cdot HCl$, DCM; (k) $Pd(OH)_2$, H_2 (65 psi), EtOH; (l) conc HCl:water (2:1), 0 °C \rightarrow rt; (m) DAST, DCM, 0 °C; (n) 1.0 N aq HCl:THF (1:1), 50 °C.

Scheme 3^a

^a Conditions: (a) Bn_2NH , EtOH, HOAc, 80 °C; (b) H_2 , Pd-C, EtOH, HOAc; (c) nitrile, MeONa, MeOH, then HOAc.

Scheme 4^a

^a Conditions: (a) Bn_2NH , EtOH, HOAc, 80 °C; (b) H_2 , Pd-C, EtOH, HOAc; (c) **19**, MeONa, MeOH, then HOAc.

Following these studies, we began a chemistry effort to examine the SAR of analogues of **3** with the intent of developing an immune modulating agent with enhanced potency and pharmacokinetics. Investigational agents were initially evaluated at 100 mg/kg by oral gavage using a 100 mg/kg dose of **3** as a positive control. Blood was drawn at 18 h after dosing and lymphocyte suppression was determined by CBC analysis. In addition to measuring *in vivo* activity by CBC, the ADME and PK profile of each analogue was established.

Analogues of **3** may be grouped broadly into three categories: (1) core heterocycle modifications, (2) tetrahy-

droxybutyl side chain manipulations, and (3) core heterocycle pendant 2-position substitutions. Other design considerations took into account the physical properties of our chemical lead. Small polar molecules like **3** often achieve plasma concentrations by paracellular absorption.²⁹ Therefore, we felt it prudent to not deviate dramatically from the physical properties of **3**, including molecular weight and polar surface area. We measured Caco-2 values and plasma protein binding (PPB) as potentially important variables on which the absorption mechanism may be dependent. With a panel of pharmacokinetic and *in vitro* ADME assays in place, we were poised to interpret the SAR of analogues prepared.

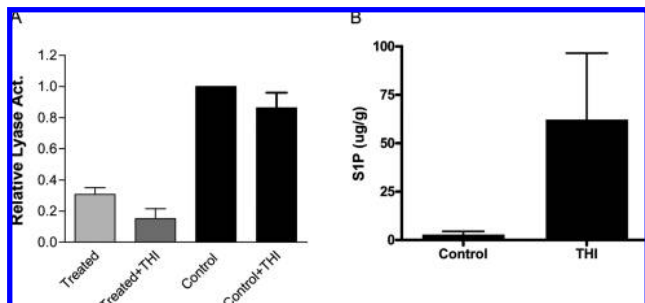


Figure 4. Residual lyase activity and SIP levels following oral administration of **3**. (A) Treated group is lysate derived from mouse spleen tissue harvested 18 h after 100 mg/kg oral administration with THI; treated + THI group is exogenous addition of THI to lysate from treated group; control group is spleen lysate from untreated mice; control + THI group is exogenous addition of THI to control group lysate. (B) SIP levels in mouse spleen lysate of control group vs SIP levels in lysate from mouse spleen tissue harvested 18 h after 100 mg/kg oral administration with THI. SIP levels measured by radioreceptor-binding assay.

Table 1. PK/PD Profile, in Vitro and Select Physical Properties of **3**

C_{max}^a	24.9	AUC^e	35.8
T_{max}^b	0.5	CL ^f	2.9
$T_{1/2}^c$	4.5	Caco-2 ^g	110
%F ^d	14	% Δ^h	-41

CC(=O)c1c[nH]c2c1C(O)C(O)CO **3**
 MW: 230 AlogP: -2.0 PSA: 127

^a Maximum exposure in (μM). ^b Time at maximum exposure (h). ^c Half-life in h. ^d Oral bioavailability calculated from 1 mg/kg iv and 10 mg/kg po. ^e Exposure calculated as $t_0 \rightarrow \text{inf}$ ($\mu\text{M}\cdot\text{h}$). Obtained from 10 mg/kg po dose to mice ($n = 5$). ^f Clearance in (mL/min/kg). Calculated from 1 mg/kg iv dose to mice ($n = 4$). ^g (nM/s), obtained at 20 μM . ^h Reported as % change in circulating lymphocytes relative to vehicle control 18 h after 100 mg/kg oral dose to mice ($n = 5$). Interanimal variability was less than 20%.

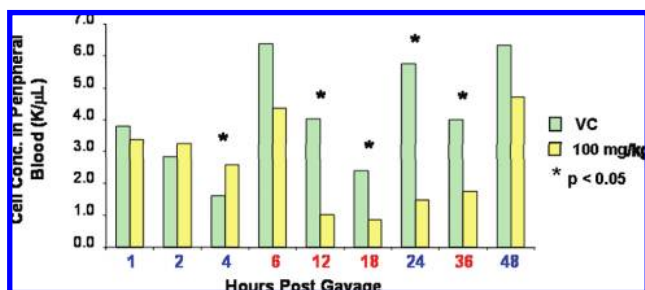


Figure 5. Time-course study of **3**. Single 100 mg/kg dose given to mice ($n = 5$) via oral gavage. Change in circulating peripheral lymphocytes for treated group (yellow) relative to vehicle control (green) at the indicated times post gavage. The modest increase in peripheral circulating lymphocytes at 4 h was deemed an experimental artifact, which occurred before the onset of pharmacology.

Core Modification SAR and PK. In vivo administration of **8** revealed that methylation at nitrogen rendered **3** inactive, as the CBC data for this analogue was comparable to vehicle control (Table 2). That the modestly improved exposure and bioavailability of imidazole **8** did not translate to an improved PD effect indicates that an N-H may be essential for intrinsic activity. Curiously, several compounds produced significantly higher levels of circulating lymphocytes. For reasons unknown to us, replacement of the central imidazole ring with thiazole **7**

Table 2. Effect of Core Modification on PK and PD

Compound	% Δ^a	AUC ^b	Caco-2 ^c	CL ^d	$T_{1/2}^e$	%F
3	-41	35.8	110	2.9	4.5	14
5	+45	43.4	134	14.0	2.1	88.0
7	+25	2.7	139	11.7	0.9	65.0
8	+10	41.1	55.7	5.7	2.4	33.6
10	-5	10.8	93.7	7.0	6.2	11.0
11	+8	6.4	79.3	17.3	2.8	17.1
12	+40	11.5	31.1	23.9	1.9	49.0

^a Reported as % change in circulating lymphocytes relative to vehicle control 18 h after 100 mg/kg oral dose of HCl salt to mice ($n = 5$). Interanimal variability was less than 20%. ^b Exposure calculated as $t_0 \rightarrow \text{inf}$ in ($\mu\text{M}\cdot\text{h}$). Obtained from 10 mg/kg po dose to mice ($n = 5$). ^c (nM/s), obtained at [20 μM]. ^d Clearance in (mL/min/kg). Calculated from 1 mg/kg iv dose to mice ($n = 4$). ^e Half-life in h. ^f Calculated from 1 mg/kg iv and 10 mg/kg po.

and pyridine **6** produced elevated lymphocyte levels. Substitution at the 5-position of the core imidazole with a range of lipophilic substituents provided data on the steric requirements in that region and allowed us to test the importance of maintaining the overall polarity of analogues. After dosing to mice, 5-alkyl analogues **10** and **11** showed diminished activity while 5-aryl analogue **12** registered elevated lymphocyte levels. Increased CL and lower exposure, possibly in addition to reduced intrinsic activity, may have contributed to lower overall in vivo potency. The incidence of compounds that elevated lymphocyte counts was low and the significance of these findings is unclear.

Side Chain Modification SAR and PK. In addition to studying the effect of core changes to **3**, we investigated the impact of changes to the composition and chirality of the hydroxylated side chain. Consequently, we were able to examine the H-bond donor-acceptor properties of the side chain. The effects of these changes are summarized in Table 3. Oral dosing of the C-4 epimer **33** revealed a moderately potent compound with reduced exposure and higher clearance relative to **3**. That the reduced oral potency of **33** correlates with reduced exposure may indicate that intrinsic potency is not significantly impacted by stereochemical inversion at C-4. More substantial side chain alterations, as presented by the enantiomer **34**, completely negated activity. Enantiomer **34** displayed a comparable pharmacokinetic profile compared to **3**, which underscores the importance of the asymmetric configuration derived from glucose. Manipulation of the side chain functional groups, as in methyl ether **36**, and tertiary amide **38**, also resulted in compounds devoid of activity. That inactive ether **36** exhibited an improved exposure points to either the importance of the

Table 3. Effect of Side Chain Modification on PK and PD

Compound	% Δ^a	AUC ^b	Caco-2 ^c	CL ^d	T _{1/2} ^e	%F
3	-41	35.8	110	2.9	4.5	14
33	-31	15.7	99	18.8	5.4	25
34	0	18.0	131	6.7	6.0	17
36	+16	42.7	---	6.8	3.3	42
38	-15	0.2	103	11.7	3.5	1

^a Reported as % change in circulating lymphocytes relative to vehicle control 18 h after 100 mg/kg oral dose of HCl salt to mice ($n = 5$). Interanimal variability was less than 20%. ^b Exposure calculated as $t_0 \rightarrow \text{inf}$ in ($\mu\text{M}\cdot\text{h}$). Obtained from 10 mg/kg po dose to mice ($n = 5$). ^c (nM/s), obtained at [20 μM]. ^d Clearance in (mL/min/kg). Calculated from 1 mg/kg iv dose to mice ($n = 4$). ^e Half-life in h. ^f Calculated from 1 mg/kg iv and 10 mg/kg po.

Table 4. Effect of 2-Substitution on PK and PD

Compound (dose)	R	% Δ^a	AUC ^b	Caco-2 ^c	CL ^d	T _{1/2} ^e	%F
3 (100 mpk)	Ac	-41	35.8	110	2.9	4.5	14
3 (30 mpk)	Ac	-25	15.0	110	2.9	2.0	12
13 (100 mpk)	CH(OH)CH ₃	-15	44.5	41	16.4	4.4	22
14 (30 mpk)	C(=NNHAc)CH ₃	-41	3.6	90	8.9	2.6	5
16 (30 mpk)	O=CNMe ₂	-11	6.7	99	11.3	4.0	5
17 (30 mpk)	CF ₂ CH ₃	-58	4.7	111	---	1.0	---
20 (30 mpk)	CF ₂ CF ₃	-11	10.0	---	1.3	1.7	31
21 (30 mpk)	O=CPh	-17	6.0	---	13.5	4.0	14

^a Reported as % change in circulating lymphocytes relative to vehicle control 18 h after indicated oral dose of HCl salt to mice ($n = 5$). Interanimal variability was less than 20%. ^b Exposure calculated as $t_0 \rightarrow \text{inf}$ in ($\mu\text{M}\cdot\text{h}$). Obtained from 10 mg/kg po dose to mice ($n = 5$). ^c (nM/s), obtained at [20 μM]. ^d Clearance in (mL/min/kg). Calculated from 1 mg/kg iv dose to mice ($n = 4$). ^e Half-life in h. ^f Calculated from 1 mg/kg iv and 10 mg/kg po.

C-3 hydroxyl in target binding or steric demands imposed by the target in this region.

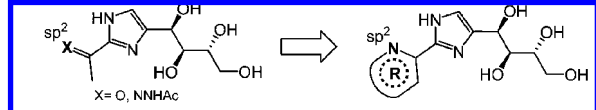
Substitution of the Imidazole 2-Position: SAR and PK Profile. Substitution at the 2-position of the imidazole also impacted in vivo activity. But, unlike modification to the side chain, some changes to the 2-position provided viable immunologic agents. The identification of compounds with enhanced activity prompted us to increase the sensitivity of our primary screen. Accordingly, we reduced of the oral dose of analogues and positive control from 100 to 30 mg/kg. (Table 4). Alcohol **13** displayed decreased potency as measured by CBC. This reduced activity was likely due to a decrease in intrinsic potency because **13** maintained a favorable PK profile. Diminished potency was observed with sterically encumbered aryl ketone **21**. The reduced potency correlated with substantially reduced exposure, potentially compounded by lower intrinsic potency.

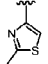
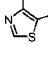
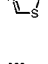

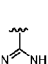
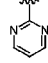
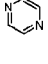

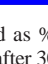
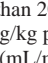
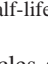
By contrast, α,α -difluoro analogue **17** displayed remarkable ability to deplete lymphocyte levels despite its low pharmacokinetic exposure. Initially, the reduced exposure was thought to be a function of a shorter half-life. However, further study of **17** in toxicokinetic (TK) experiments revealed significant toxicity when dosed to mice orally at 100 mg/kg. Concurrent with PK and toxicology experiments were chemical observations made during the synthesis of similarly substituted α,α -difluoro analogues. While our final products were clearly stable during characterization, hydrolysis products were observed during purification. We determined that acid-catalyzed hydrolysis of α,α -difluoro analogue **17** regenerated the parent ketone with liberation of 2 equiv of HF.³⁰ This observation clarified the short half-life of **17** and left little doubt regarding the nature of the toxicity observed in the mouse TK experiments. In fact, subsequent pathology confirmed findings consistent with HF poisoning.³¹

Acylhydrazone **14** gave early indications of enhanced activity relative to **3** despite its lower exposure. Cognizant of potential chemical stability issues, we reasoned that the low exposure may relate to the sensitivity of the acylhydrazone group to the acidic conditions present in the upper gastrointestinal tract. Despite the lower concentrations of parent compound measured in the plasma, we observed an increase in intrinsic potency over **3**. Given our SAR at the 2-position, it was postulated that the H-bond acceptor capacity of the Lewis-basic carbonyl oxygen was essential to the potency of investigational agents. We hypothesized that the C=N carbonyl of acylhydrazone **14** functioned as a ketone equivalent and that potency may extend to other sp^2 hybridized nitrogens in this region of the molecule. We reasoned that heterocycles containing an appropriately oriented C=N bond within the ring could also function as a ketone surrogate. Consequently, we prepared and evaluated a diverse series of analogues bearing heterocycles at the pendant 2-position of the parent imidazole ring.

2-Heterocycle SAR and PK. Having identified the 2-position of the central imidazole as an area tolerant to structural modification, a series of 2-heterocycles bearing a basic nitrogen proximal to the imidazole ring were synthesized. Commercial availability of a wide variety of heterocyclic nitriles, or nitrile precursors, made a thorough investigation of this SAR possible. Data within Table 5 confirm that a C=O carbonyl, a C=N carbonyl, or a structural homologue at the 2-position is a common feature among active analogues.

As shown in Table 5, thiazoles **22**, **23**, and **24** exhibited a range of in vivo activity. The unsubstituted thiazole **24** displayed significant in vivo potency over the substituted thiazoles **22** and **23**. That *N*-methylimidazole **32** lacks potency suggests a steric constraint in this region of the molecule. Interestingly, the opposite trend emerges with triazoles **26** and **27**. *N*-Benzyl triazole **26** was active while unsubstituted triazole **27** lacked potency. This trend may reflect the preference for lipophilic substituents in this region. Alternatively, heteroatoms in this region may not be tolerated. The latter hypothesis is supported by the difference in potency between pyrimidine **29** and pyrazine **30**. We were pleasantly surprised to discover that imidazole **28** induced particularly significant lymphopenia when administered orally at 30 mg/kg to mice. While our hypothesis concerning the importance of a sp^2 hybridized nitrogen was generally consistent with these data, some exceptions exist. For example, the unsubstituted oxazole **25** proved to be inactive despite the close structural resemblance to thiazole **24**. Oxadiazole **31** displayed only moderate activity in our assay. It is worth noting that, despite showing lower exposure relative to **3**, several

Table 5. Effect of 2-Heterocycle Carbonyl Replacements (30 mg/kg) on PK and PD^d


Compound	R	% Δ ^a	AUC ^b	Caco-2 ^c	CL ^d	T _{1/2} ^e	%F
3		-25	15.0	110	2.9	2.0	12
22		0	6.9	199	19.4	2.1	23
23		-7	—	49	—	—	—
24		-33	5.8	0	12.7	4.2	12
25		+1	3.4	9	16.6	1.2	—
26		-41	1.7	51	16.4	2.4	6
27		+7	—	10	—	—	—
28		-53	5.9	259	31.5	3.2	28
29		-26	3.0	109	15.2	2.4	7
30		-6	4.7	198	13.4	1.9	10
31		-16	3.2	141	11.3	0.7	5
32		-5	2.6	262	9.1	1.6	3

^a Reported as % change in circulating lymphocytes relative to vehicle control 18 h after 30 mg/kg oral dose of HCl salt to mice ($n = 5$). Interanimal variability was less than 20%. ^b Exposure calculated as $t_0 \rightarrow \text{inf}$ in ($\mu\text{M} \cdot \text{h}$). Obtained from 10 mg/kg po dose to mice ($n = 5$). ^c (nM/s), obtained at [20 μM]. ^d Clearance in (mL/min/kg). Calculated from 1 mg/kg iv dose to mice ($n = 4$). ^e Half-life in h. ^f Calculated from 1 mg/kg iv and 10 mg/kg po.

2-heterocycles showed equivalent and even superior potency. That this biological activity was achieved with 2-heterocycles **24**, **26**, **28**, and **29** may suggest that superior target affinity compensates for impaired pharmacokinetics. Alternatively, these analogues may better address the unresolved mechanistic subtleties of the interaction between **3** and S1PL (e.g., involvement of a higher-order complex). Another subtlety involves other mechanism(s) that may also contribute to the antiinflammatory activity of S1PL inhibition beyond simply limiting lymphocyte egress. While establishing the precise mechanism remains a priority, our medicinal chemistry efforts have identified compounds with improved efficacy in models of autoimmune disease and these results will be the subject of future reports.

Conclusions

Inhibition of S1PL correlates with increased concentrations of S1P in lymphoid tissue, resulting in decreased levels of peripherally circulating lymphocytes, and shows therapeutic potential for the control of autoimmune disease. The pharmacology observed after administration of **3** is strikingly similar in many respects to the phenotype of genetically altered mice expressing reduced levels of S1PL. While **3** does not show direct inhibition of S1PL *in vitro*, oral administration clearly correlates with reduced lyase activity in lymphoid tissue concomitant with elevated levels of S1P. Evidently, S1PL inhibition triggered by **3** involves a more complicated scenario than inhibition by a discrete binary ligand–protein complex. Further elucidation of this mechanism of action remains a priority. Alterations to the side chain and core heterocycle reduced the potency of

analogues of **3**, as did several transformations at the pendant ketone. By contrast, compounds bearing certain heterocycles at the 2-position of the imidazole core provided superior *in vivo* activity. Ongoing efforts targeting S1PL by direct *in vivo* evaluation of synthetic analogues of **3** has led to the discovery of clinically useful compounds. Efficacy studies in animal models of autoimmune disease and human data from clinical trials will be the subject of future reports.

Experimental Procedures

Animal Handling and In Vivo Methods. All procedures were conducted according to applicable standard operating procedures and with the approval of the Lexicon Pharmaceuticals Incorporated institutional animal care and usage committee. The tested analogues were formulated in sterile water and dosed to 129/SvEvBrd \times C57BL/6 F1 mice. The pH of intravenous dosing solution was adjusted to between 5 and 6 and between 3 and 4 for oral administration. The intravenous dose volume was 3.7 mL/kg body weight and the oral gavage volume was 5 mL/kg body weight at 1 and 10 mg/kg body weight, respectively. Animals were observed regularly throughout the day on days in which they were dosed, and these clinical observations were recorded. For the purpose of exposure, blood was collected using saphenous vein bleeds in unanaesthetized animals, except for terminal bleeds, which were performed using cardiac puncture immediately following euthanasia. Blood samples were collected at 0.08, 0.25, 0.5, 1, 3, and 6 h post intravenous dosing and at 0.25, 0.5, 1, 2, 4, 6, and 24 h post oral administrations. An aliquot of 25 μL of blood in K₂-EDTA tubes was spun following each time point, and 10 μL of the resulting plasma was transferred to fresh polypropylene tubes for exposure assessment by liquid chromatography–mass spectrometry.

Measurement of S1PL Activity. Spleens of mice were homogenized in ice-cold buffer containing 50 mM KPO₄, pH 7.5, 1 mM EGTA, 1 mM DTT, and complete protease inhibitor cocktail (Roche Applied Science, Indianapolis, IN). The homogenate was centrifuged at 2500g for 10 min, and the supernatant was used for enzyme activity measurements. Protein concentration was determined using the Bradford assay. S1PL activity was determined using ³³P-labeled S1P as substrate (American Radiolabeled Chemicals, St. Louis, MO). The reactions were carried out in a 50 μL volume containing 100 mM KPO₄, pH 7.4, 1 mM EDTA, 25 mM NaF, 5 mM DTT, phosphatase inhibitors I and II (Sigma-Aldrich), 0.1% Triton X-100, and various amounts of tissue lysate. The reactions were initiated by addition of pyridoxal phosphate (final concentration 50 μM) and 15 nCi of [³³P]-S1P (specific activity 0.66 Ci/mmol, total S1P concentration 0.5 μM). The reaction mixtures were incubated at 37 °C for 1 h and terminated with the addition of 90 μL of 35% acetonitrile containing 0.1% TFA. Then 120 μL of the mixtures were then transferred to a 96-well C18 multi-SPE plate (Millipore Corporation, Bedford, MA) pre-equilibrated first with 100 μL of MeOH and then with 200 μL of 20% acetonitrile containing 0.1% TFA. The plate was briefly centrifuged at 3000 rpm for 1 min, and the filtrate was collected and assayed for ³³P activity by scintillation counting.

Measurement of S1P Concentration. S1P extraction from mouse sera was performed by mixing 100 μL of serum with 900 μL MeOH containing 0.1% TFA in an Eppendorf tube. After vortexing for 2 min, 800 μL of water with 0.1% TFA was added to the samples. Then, 300 μL of the mixture was then transferred to a 96-well C18 multi-SPE plate pre-equilibrated first with 100 μL of MeOH and then with 200 μL of 20% acetonitrile containing 0.1% TFA. The plates were spun at 3000 rpm for 1 min and the bound S1P eluted in 100 μL of MeOH. The eluate was dried and stored at 4 °C overnight before analysis. S1P extraction from single cell suspensions of mouse splenocytes was performed by using $4\text{--}6 \times 10^7$ cells. Cells were washed with ice-cold PBS and resuspended by vortexing for 2 min in 500 μL of MeOH containing 0.1% TFA. Then 500 μL of water with 0.1% TFA was added to the samples and S1P was eluted and dried as described for the serum samples, using 160 μL mixture/well on a C18 multi-SPE plate. S1P levels

in the eluates were measured with a whole cell receptor binding assay using HEK293 cells expressing the S1P1 (Edg1) receptor. Five $\times 10^4$ HEK293-S1P1 cells/well were seeded into clear bottom 96-well plates coated with poly-D-lysine (BD BioSciences) and incubated overnight at 37 °C. Cells were placed on ice for 15 min then washed twice with ice-cold binding buffer (25 mM Tris-HCl, pH 7.5, 100 mM NaCl, 50 mM NaF, 0.4% fatty acid free BSA, fraction 5). Dried S1P eluates or standards were resuspended in 50 μ L of ice-cold binding buffer containing 25000 cpm [33 P]-S1P (specific activity 0.6 Ci/mmol) and incubated on ice for 60 min. After washing twice with 100 μ L of ice-cold binding buffer, 50 μ L of lysis buffer (0.1% SDS, 0.4% NaOH, 2% Na₂CO₃) was added and the plates were shaken for 5 min. Then 40 μ L of cell extract was then transferred to a white opaque microplate (Costar, Cambridge, MA, cat. no. 3912) and counted after the addition of 120 μ L of MS 40 microscint. S1P content of extracts was estimated from standard curves (between 42 pM and 2.5 μ M), generated with cold S1P.

Chemical Methods. All reactions were conducted under a static atmosphere of argon or nitrogen and stirred magnetically unless otherwise noted. Reagents, starting materials, and solvents were purchased from commercial suppliers and used as received. Flash column chromatography was carried out using prepacked silica gel columns from Biotage or ISCO or by slurry preparation using EMD silica gel 60 (particle size 0.040–0.063 mm). ¹H and ¹³C NMR spectra were collected on Bruker ARX300, DRX400, or DPX400, or Varian Mercury 400 MHz NMR spectrometers. Chemical shifts are reported in parts per million (ppm) relative to tetramethylsilane in δ units, and coupling constants (*J* values) are given in hertz (Hz). Data are reported in the following format: chemical shift, multiplicity, coupling constants, and assignment. Reactions were monitored by TLC using 0.25 mm E. Merck silica gel plates (60 F₂₅₄) and were visualized with UV light. Analytical HPLC spectra were collected on Shimadzu HPLC systems equipped with a UV detector measuring absorbance at 220 and 254 nm. Mass spectra were obtained on Waters ZQ or ZMD LCMS systems equipped with an autosampler, an ELSD detector, a UV detector measuring absorbance at 220 and 254 nm, and a mass detector. High-resolution mass spectra were obtained on a Waters LCT Premier XE Micromass MS Technologies instrument equipped with an autosampler. Elemental analysis was conducted by Robertson Microlit Laboratory, Madison, NJ.

2-Ethoxyacrylonitrile (19). A 250 mL jacketed three-neck round-bottom flask was equipped with a magnetic stir bar, rubber septum with temperature probe, plastic stopper, and pressure-equalized addition funnel with gas bubbler. The vessel was charged with bromoacetaldehyde diethylacetal (35.33 g, 179.28 mmol) and tin(II) chloride (167 mg, 0.88 mmol). The suspension was cooled to 3 °C before the addition of trimethylsilyl cyanide (17.69 g, 178.31 mmol) over 15 min, while maintaining the reaction temperature below 15 °C. The mixture was held at about 10 °C for 30 min, then warmed to 20 °C for 2 h or until GC analysis showed consumption of bromoacetaldehyde diethylacetal. The resulting yellow solution was diluted with MTBE (85 mL). Diethylamine (19.61 g, 268.11 mmol) was added over 10 min while the temperature was maintained below 35 °C. The resulting thick slurry was diluted with additional portion of MTBE (25 mL). The reaction mixture was stirred at about 25 °C for 2 h or until reaction was complete as determined by GC analysis. The mixture was filtered and the collected solids were washed MTBE (2 \times 30 mL). The combined filtrate was concentrated under vacuum. The resulting crude ethoxyacrylonitrile was polish-filtered and vacuum distilled to give **19** as a clear liquid (11.2 g, 67% yield); bp: 46–49 °C/31 mmHg. ¹H NMR (400 MHz, CDCl₃) δ ppm 4.85 (d, *J* = 3.54 Hz, 1H), 4.75 (d, *J* = 3.28 Hz, 1H), 3.73 (q, *J* = 6.99 Hz, 2H), 1.24 (t, *J* = 6.95 Hz, 3H). ¹³C NMR (100 MHz, CDCl₃) δ ppm 136.58, 115.23, 101.11, 65.54, 14.40.

General Procedure A: Fructosamine-HOAc (18). A 12 L three-neck round-bottom flask with mechanical stirrer, rubber septum with temperature probe, and reflux condenser with gas bubbler was charged with D-(+)-glucose (504.08 g, 2.798 mol), absolute ethanol

(2.7 L), dibenzylamine (539.14 g, 2.733 mol), and glacial acetic acid (160 mL, 2.795 mol). The suspension was set stirring under nitrogen and heated to reflux. After 4 h, the reaction was allowed to gradually cool to room temperature and stirred under nitrogen overnight. The resulting suspension was filtered, and the solids were washed with ethanol (2 \times 750 mL) and heptane (500 mL). The filter cake was dried under vacuum at 50 °C overnight to afford a white solid (923 g). A 12 L three-neck round-bottom flask with mechanical stirrer, subsurface gas inlet bubbler, and gas outlet tube was charged with a portion of this solid (219.50 g, 610.71 mmol), ethanol (3.0 L), and acetic acid (1.5 L). The resulting suspension was sparged with nitrogen for 30 min and then treated with 10% Pd/C DeGussa type, 50 wt % water (44.47 g, 2.22 g active Pd). Hydrogen was bubbled into the stirring mixture for 4 h then sparged with nitrogen for 30 min, and the product solids were dissolved upon addition of water (800 mL). The resulting solution was filtered through to remove insoluble catalyst solids, and the yellow filtrate was concentrated under vacuum to give a tan solid, which was dissolved in water (150 mL) warmed to 55 °C. Ethanol (1.0 L) was added over 5 min to the warm solution to provide a turbid solution, which formed a suspension upon standing. The thickening suspension was let stand at 55 °C for 15 min, then gradually cooled to room temperature while stirring. The suspended solids were filtered and filter cake was washed with 2-propanol (2 \times 250 mL) and heptane (1 \times 250 mL) and then were dried in a vacuum oven to afford fructosamine-HOAc **18** (124.16 g, 85% yield) as a fine off-white chalky powder. Characterization of the obtained material was in good agreement with literature values.³²

General Procedure B: 1-(4-((1R,2S,3R)-1,2,3,4-Tetrahydroxybutyl)-1H-imidazol-2-yl)ethanone (THI, 3). To a three-neck, 12 L round-bottom flask equipped with a mechanical stirrer and a temperature controller was added ethoxyacrylonitrile (10.0 g, 103.0 mmol) and methanol (200 mL). The solution was treated with 25 wt % sodium methoxide in methanol (14.1 mL, 60.0 mmol) and maintained at room temperature for 1 h. Then, fructosamine-HOAc (23.9 g, 100.0 mmol) was added in one portion, and the slurry was stirred at room temperature for 6 h. Then another portion of 25 wt % sodium methoxide in methanol (11.8 mL, 50.0 mmol) was added and the reaction was maintained at room temperature for 16 h. The mixture was then diluted with water (200 mL) and treated with acetic acid (11.8 mL, 200.0 mmol). After stirring at 60 °C for 1 h, the solution was concentrated to 100 mL total volume. The slurry was cooled to 0 °C and stirred for 1 h then filtered and the solids were washed with water (2 \times 10 mL). The solids were collected and dried under vacuum at 50 °C to afford a pale-yellow solid, which was slurried in water (100 mL) and heated to boiling for 15 min before cooling to 0 °C. The mixture was stirred for 1 h then filtered, and the solids were washed with water (2 \times 10 mL) and dried to constant weight in a vacuum oven at 50 °C to provide **3** (19.5 g, 82% yield) as a pale-yellow solid. The product was analytically pure but may be purified further by recrystallization from MeOH/Et₂O or by precipitating from water upon treatment with 2.0 M aq NaOH solution. ¹H NMR (400 MHz, 1.0 M HCl in D₂O) δ ppm 7.48 (d, *J* = 2.0 Hz, 1 H), 5.09 (s, 1 H), 3.40–3.70 (m, 4H), 2.53 (d, *J* = 2.4 Hz, 3H). ¹³C NMR (400 MHz, 1.0 M HCl in D₂O) δ ppm 185.0, 139.4, 138.0, 119.5, 73.0, 70.9, 65.0, 63.2, 26.7. MS (EI) *m/z*: 231 [M + H]⁺. HRMS calcd for C₂₂H₁₅N₂O₅ [M + H]⁺ 231.0981, found 231.0976. HPLC (Zorbax C8 4.6 mm \times 150 mm, 4% MeCN:10 mM aq NH₄OAc, 4 min isocratic) *t*_R = 1.11 min, 100% integrated area.

1-(6-((1R,2S,3R)-1,2,3,4-Tetrahydroxybutyl)pyridin-2-yl)ethanone (5). 2-Bromo-6-(2-methyl-1,3-dioxolan-2-yl)pyridine **4**³³ (3.97 g, 16.30 mmol) was suspended in THF (120 mL) and cooled to –78 °C. *n*-Butyl lithium (1.6 M in hexanes, 12.2 mL) was added dropwise, and the reaction was warmed to –40 °C for 45 min. The reaction was recooled to –78 °C, and a solution of 3,4-*O*-isopropylidene-D-erythronolactone (4.64 g, 29.3 mmol) in THF (40 mL) was added dropwise over 30 min. After stirring for 2 h, the reaction was quenched with sat. aq NH₄Cl (50 mL). The reaction was warmed to room temperature and then extracted with EtOAc (3 \times 50 mL). The combined organic portions were washed with

water (50 mL) and brine (30 mL) and then dried over MgO₄, filtered, and concentrated to provide a yellow solid, which was used without further purification. To a -60 °C solution of the intermediate lactol (2.77 g, 8.57 mmol) in isopropyl alcohol (248 mL) was added solid sodium borohydride (3.24 g, 85.7 mmol) portionwise over 20 min. The reaction was removed from the cold bath and stirred overnight. The reaction was then concentrated and the residue diluted with brine (100 mL) and extracted with EtOAc (3 × 100 mL). The combined organics were dried over MgO₄, then filtered and concentrated to provide a crude mixture of diastereomers, which were separated by preparative HPLC. The desired diastereomer (0.53 g, 1.64 mmol) was taken up in 1:1 acetone:water (50 mL), treated with conc HCl (14 mL), and the reaction was heated to 80 °C for 2 h. At completion, the acetone was removed under vacuum, and the remaining aqueous portion washed with ether (3 × 50 mL). The aqueous portion was concentrated and then purified by HPLC to provide **5** (0.18 g, 8% yield, 3 steps) as a white solid. The absolute configuration at the benzylic center was confirmed by single crystal X-ray analysis. ¹H NMR (400 MHz, 1.0 M HCl in D₂O) δ ppm 7.85–8.09 (m, 2 H), 7.74 (d, *J* = 7.6 Hz, 1 H), 5.10 (d, *J* = 2.3 Hz, 1 H), 3.94 (dd, *J* = 8.2, 2.4 Hz, 1 H), 3.76–3.87 (m, 2 H), 3.63 (dd, *J* = 11.6, 6.3 Hz, 1 H), 2.70 (s, 3 H). ¹³C NMR (100 MHz, 1.0 M HCl in D₂O) δ ppm 203.94, 160.89, 152.13, 139.05, 125.95, 122.29, 74.24, 72.66, 71.61, 63.39, 26.15. MS (EI) *m/z*: 242 [M + H]⁺; mp: 142–144 °C. HRMS calcd for C₁₁H₁₅NO₅ [M + H]⁺ 242.1028, found 242.1019. HPLC (Zorbax C8 4.6 mm × 150 mm, 10–90% MeCN:10 mM aq NH₄OAc, 3 min gradient) *t*_R = 1.72 min, 100% integrated area.

1-(1-Methyl-4-((1R,2S,3R)-1,2,3,4-tetrahydroxybutyl)-1H-imidazol-2-yl)ethanone (8). To a room temperature slurry of **3** (190 mg, 0.83 mmol) and K₂CO₃ (229 mg, 1.66 mmol) in DMF (5 mL) was added MeI (56 μL, 0.91 mmol). After 4 h, the reaction was filtered and concentrated and then purified by HPLC. Pure fractions were combined and concentrated and then suspended in water (5 mL) and lyophilized to afford **8** (121 mg, 60% yield) as a white powder. ¹H NMR (400 MHz, MeOD) δ ppm 7.19 (s, 1 H), 4.86 (s, 1 H), 3.86 (s, 3 H), 3.61–3.75 (m, 3 H), 3.55 (dd, *J* = 13.6, 5.3 Hz, 1 H), 2.44–2.49 (m, 3 H). ¹³C NMR (100 MHz, MeOD) δ ppm 191.61, 145.23, 143.42, 126.99, 75.52, 73.14, 69.06, 65.09, 36.70, 27.31. Regiochemistry of *N*-methylation determined by NOE between *N*-CH₃ and *Ar-H*. MS (EI) *m/z*: 245 [M + H]⁺. HRMS calcd for C₁₀H₁₆N₂O₅ [M + H]⁺ 245.1137, found 245.1120. HPLC (C30 Develosil RP Aqueous 4.6 mm × 50 mm, 5–50% [methanol/water/TFA (95/5/0.1)]:water, 4 min gradient) *t*_R = 1.52 min, 99% integrated area.

1-(5-Bromo-4-((4S,4'R,5R)-2,2,2'-tetramethyl-4,4'-bi(1,3-dioxolan)-5-yl)-1H-imidazol-2-yl)ethanone (9). To a round-bottom flask charged with THI (11.00 g, 47.61 mmol) suspended in dichloroethane (100 mL) was added 2,2-dimethoxypropane (100 mL) and *p*-toluenesulfonic acid (1.84 g, 9.60 mmol). The mixture was heated to 50 °C for 24 h. At completion, the resulting solution was neutralized with triethylamine (5 mL), washed with water (2 × 100 mL) and brine (100 mL), and then dried over MgO₄, filtered, and concentrated to provide the intermediate THI-bisketal (12.01 g, 81% yield) as a clear yellow plastic mass. ¹H NMR (400 MHz, chloroform-*d*) δ ppm 10.54–11.31 (m, 1 H), 7.24 (s, 1 H), 5.00 (d, *J* = 7.5 Hz, 1 H), 4.08–4.30 (m, 3 H), 3.94–4.03 (m, 1 H), 2.59–2.66 (m, 3 H), 1.43–1.51 (m, 6 H), 1.26–1.42 (m, 6 H). MS (EI) *m/z*: 311 [M + H]⁺. HRMS calcd for C₂₂H₁₅N₂O₅ [M + H]⁺ 311.1607, found 311.1579.

To solution of the intermediate THI-bisketal (6.23 g, 20.00 mmol) in DCM (100 mL) was added a 2.0 M solution of aqueous Na₂CO₃ (100 mL). The rapidly stirring biphasic mixture was cooled to 0 °C and then treated with bromine (3.36 g, 21.00 mmol) dropwise. The cold bath was removed, and the mixture was maintained for 10 min. At completion, the layers were separated and the aqueous phase was washed with DCM (100 mL). The combined organics were washed with brine (100 mL), dried over MgO₄, and then filtered and concentrated. The crude material was purified by flash chromatography over silica gel (5% MeOH:DCM eluent) to provide bromide **9** (7.24 g, 93% yield) as a white solid. ¹H NMR (400

MHz, chloroform-*d*) δ ppm 11.03 (br s, 1 H), 5.03 (d, *J* = 8.1 Hz, 1 H), 4.11–4.24 (m, 2 H), 3.99–4.07 (m, 1 H), 3.95 (dd, *J* = 8.6, 4.5 Hz, 1 H), 2.64 (s, 3 H), 1.52 (s, 3 H), 1.48 (s, 3 H), 1.33 (s, 3 H), 1.22 (s, 3 H). ¹³C NMR (100 MHz, chloroform-*d*) δ ppm 189.08, 144.12, 129.77, 117.03, 111.09, 110.21, 81.11, 76.47, 73.64, 67.42, 26.98, 26.92, 26.45, 25.48, 25.26. MS (EI) *m/z*: 389, 391 [M + H]⁺. HRMS calcd for C₁₅H₂₁BrN₂O₅ [M + H]⁺ 389.0712, found 389.0753.

General Procedure C: 1-(5-Methyl-4-((1R,2S,3R)-1,2,3,4-tetrahydroxybutyl)-1H-imidazol-2-yl)ethanone (10). To a solution of the bromide **9** (1.12 g, 2.88 mmol) in toluene (12 mL) and DMF (6 mL) was added cesium fluoride (875 mg, 5.76 mmol), Pd(dppf)Cl₂ (118 mg, 0.144 mmol), and methyl boronic acid (346 mg, 5.76 mmol). The resulting slurry was iteratively evacuated and then backfilled with nitrogen while sonicating for 15 min and then heated to 100 °C for 16 h. At completion, the reaction was filtered over a pad of celite. The filter pad was washed with toluene (2 × 10 mL), and the combined organics were concentrated and then dried under vacuum. The crude material was purified by flash chromatography over silica gel (30–50% EtOAc:hexanes eluent) to provide a plastic mass that was dissolved acetone (6 mL) and water (6 mL) and treated with concentrated HCl (2 mL). The reaction was maintained at room temperature for 2 h. At completion, the reaction was concentrated and then dissolved in water (5 mL) and lyophilized to provide **10** (84 mg, 27% yield, 2 steps) as a white powder. ¹H NMR (300 MHz, 1.0 M DCl in D₂O) δ ppm 4.83 (d, *J* = 1.5 Hz, 1 H), 3.49–3.64 (m, 3 H), 3.43 (dd, *J* = 11.3, 6.7 Hz, 1 H), 2.43 (s, 3 H), 2.19 (s, 3 H). MS (EI) *m/z*: 245 [M + H]⁺. HRMS calcd for C₁₀H₁₆N₂O₅ [M + H]⁺ 245.1137, found 245.1131. HPLC (C30 Develosil RP Aqueous 4.6 mm × 50 mm, 10–95% [methanol/water/TFA (95/5/0.1)]:water, 4 min gradient) *t*_R = 1.35 min, 97% integrated area.

1-(5-Ethyl-4-((1R,2S,3R)-1,2,3,4-tetrahydroxybutyl)-1H-imidazol-2-yl)ethanone (11). General procedure C was applied to bromimidazole **9** (1.26 g, 3.25 mmol) with vinylboronic acid pinacol ester (1.00 g, 6.49 mmol, 2.00 equiv), Pd(dppf)Cl₂-DCM (133 mg, 0.163 mmol), and cesium fluoride (1.14 g, 7.50 mmol). After purification by flash chromatography (20–40% EtOAc:hexanes eluent), the intermediate was dissolved in ethanol (10 mL), treated with 10 wt % Pd-C (100 mg), and maintained under hydrogen (1 atm) for 1 h. At completion, the reaction was sparged with nitrogen, filtered, and concentrated. Subsequent ketal deprotection by general method C provided **11** (454 mg, 54% yield, 3 steps) as a white solid. ¹H NMR (400 MHz, 1.0 M DCl in D₂O) δ ppm 5.09 (d, *J* = 2.7 Hz, 1 H), 3.57–3.72 (m, 2 H), 3.42–3.54 (m, 2 H), 2.63 (q, *J* = 7.7 Hz, 2 H), 2.44–2.55 (m, 3 H), 1.02–1.14 (m, 3 H). MS (EI) *m/z*: 259 [M + H]⁺. HRMS calcd for C₁₁H₁₈N₂O₅ [M + H]⁺ 259.1294, found 259.1284. HPLC (Zorbax C8 4.6 mm × 150 mm, 5–20% [methanol/water/TFA (95/5/0.1)]:water with 0.1% TFA, 6 min gradient) *t*_R = 3.34 min, 99% integrated area.

1-(5-Phenyl-4-((1R,2S,3R)-1,2,3,4-tetrahydroxybutyl)-1H-imidazol-2-yl)ethanone (12). General procedure C was applied to bromimidazole **9** (778 mg, 2.00 mmol) using phenylboronic acid (488 mg, 4.00 mmol), Pd(dppf)Cl₂-DCM (82 mg, 0.10 mmol, 0.05 equiv), and cesium fluoride (603 mg, 4.00 mmol). After purification by flash chromatography (10–30% EtOAc:hexane), ketal deprotection provided **12** (288 mg, 47% yield, 2 steps) as a white powder. ¹H NMR (400 MHz, 1.0 M DCl in D₂O) δ ppm 7.36–7.50 (m, 5 H), 5.16 (d, *J* = 2.0 Hz, 1 H), 3.46–3.62 (m, 3 H), 3.37 (dd, *J* = 11.7, 5.9 Hz, 1 H), 2.56 (s, 3 H). MS (EI) *m/z*: 307 [M + H]⁺. HRMS calcd for C₁₅H₁₈N₂O₅ [M + H]⁺ 307.1294, found 307.1282. HPLC (Zorbax C8 4.6 mm × 150 mm, 10–90% MeCN:10 mM aq NH₄OAc, 3 min gradient) *t*_R = 2.42 min, 97% integrated area.

(1R,2S,3R)-1-(2-(1-Hydroxyethyl)-1H-imidazol-4-yl)butane-1,2,3,4-tetraol (13). To a room temperature slurry of **3** (230 mg, 1.00 mmol) in MeOH (10 mL) was added granular sodium borohydride (189 mg, 5.00 mmol). The reaction was maintained at room temperature overnight. The reaction then was cooled to 0 °C, treated with 1 N aqueous HCl solution (20 mL), and allowed to warm to room temperature for 1 h before concentration. The resulting paste was diluted with water (5 mL) and then adjusted to pH ~9 with 1 N aq

NaOH and allowed to stand overnight in a +4 °C refrigerator. The resulting precipitant was filtered and washed with cold water (5 mL). The solid was treated with 1 N aqueous HCl solution (1 mL) and water (2 mL), then lyophilized to provide the alcohol **13** (115 mg, 50% yield) as a white solid. ¹H NMR (400 MHz, 1.0 M DCl in D₂O) δ ppm 7.21 (s, 1 H), 5.07 (q, *J* = 6.8 Hz, 1 H), 5.02 (s, 1 H), 3.48–3.74 (m, 4 H), 1.47 (s, 3 H). MS (EI) *m/z*: 233 [M + H]⁺. HRMS calcd for C₉H₁₆N₂O₅ [M + H]⁺ 233.1137, found 233.1137. HPLC (Zorbax C8 4.6 mm × 150 mm, 5–40% methanol with 0.1% TFA:water with 0.1% TFA, 5 min) *t*_R = 2.76 min, 100% integrated area.

(E)-N'-(1-(4-((1R,2S,3R)-1,2,3,4-Tetrahydroxybutyl)-1H-imidazol-2-yl)ethylidene)acetohydrazide (14). To a room temperature suspension of **3** (160 mg, 0.70 mmol) in methanol (3 mL) and water (1 mL) was added acetic hydrazide (56 mg, 0.75 mmol) and concentrated aqueous hydrochloric acid (50 μL). The suspension was stirred at 50 °C for 24 h, and the resulting solution was cooled to room temperature and then diluted with tetrahydrofuran (10 mL). A white precipitate was collected and washed with tetrahydrofuran to yield the **14** (129 mg, 65% yield) as a white solid. ¹H NMR (400 MHz, DMSO-*d*₆) δ ppm 2.2 (s, 3H), 2.5 (s, 3H) 3.4–3.7 (m, 4H), 4.3 (m, 2H), 4.6–5.0 (m, 4H), 7.0 (m, 1H), 10.30 (s, 1H), 10.37 (s, 1H). ¹³C NMR (100 MHz, DMSO-*d*₆) δ ppm 172.78, 165.91, 144.49, 143.77, 140.50, 74.00, 73.89, 71.29, 63.45, 20.71, 12.50. MS (EI) *m/z*: 287 [M + H]⁺. HRMS calcd for C₁₁H₁₈N₄O₅ [M + H]⁺ 287.1355, found 287.1360. HPLC (C30 Develosil RP Aqueous 4.6 mm × 50 mm, 8–40% [methanol/water/TFA (95/5/0.1)]:water with 0.1% TFA, 5 min gradient) *t*_R = 0.23 min, 100% integrated area.

1-Benzyl-4-((4S,4'R,5R)-2,2,2',2'-tetramethyl-4,4'-bi(1,3-dioxolan-5-yl)-1H-imidazole-2-carboxylic Acid (15). To a room temperature solution of THI-bisketal (see preparation of **9**) (20.0 g, 64.5 mmol) in DMF (200 mL) was added K₂CO₃ (12.5 g, 90.3 mmol) and benzyl bromide (10.7 mL, 90.3 mmol). The reaction was heated at 50 °C for 18 h. Then, an additional portion of benzyl bromide (5 mL, 42.0 mmol) was added and the temperature was increased to 60 °C. After 3 h, the reaction was quenched with water (200 mL), cooled to 0 °C, and extracted with EtOAc (3 × 200 mL). The organic extracts were washed with water (200 mL) and then brine (100 mL) and dried over sodium sulfate. After concentration, flash chromatography (20–40% EtOAc:hexane eluent) provided the fully protected intermediate (16.10 g, 62% yield) as a plastic mass that was used without further purification. ¹H NMR (400 MHz, chloroform-*d*) δ ppm 7.25–7.38 (m, 4 H), 7.18 (dd, *J* = 7.6, 1.8 Hz, 2 H), 5.58 (d, *J* = 5.8 Hz, 2 H), 4.92 (d, *J* = 7.8 Hz, 1 H), 4.35 (dd, *J* = 7.6, 6.8 Hz, 1 H), 4.25 (dd, *J* = 17.7, 6.3 Hz, 1 H), 4.10 (dd, *J* = 8.6, 6.3 Hz, 1 H), 4.01 (dd, *J* = 8.6, 4.8 Hz, 1 H), 2.65 (s, 3 H), 1.50 (d, *J* = 16.7 Hz, 6 H), 1.27 (m, 6 H). ¹³C NMR (100 MHz, chloroform-*d*) δ ppm 142.64, 140.44, 136.48, 129.01, 128.29, 127.88, 127.10, 124.52, 110.16, 109.71, 80.69, 75.52, 66.88, 52.00, 27.58, 27.22, 27.12, 26.54, 25.42.

A portion of the product obtained above (13.00 g, 32.50 mmol) was dissolved in dioxane (120 mL) and treated with NaOH (13.20 g, 33.00 mmol) dissolved in commercial bleach (200 mL, 6% NaOCl). After 2 h of vigorous stirring, the layers were separated and the aqueous layer was washed with EtOAc (3 × 150 mL). The combined organic extracts were washed with brine (2 × 100 mL) and then dried over celite. Filtration and evaporation afforded a solid that was further dried in vacuo to afford the carboxylic acid **15** (13.0 g, 100% yield) as a white solid. ¹H NMR (400 MHz, MeOD) δ ppm 7.10–7.45 (m, 1 H) 5.05 (br s, 1 H) 3.72–3.93 (m, 2 H) 3.66 (dd, *J* = 10.7, 4.9 Hz, 2 H) 3.06 (br s, 1 H) 1.11–1.17 (m, 2 H) 1.05–1.11 (m, 2 H). MS (EI) *m/z*: 403 [M + H]⁺.

N,N-Dimethyl-4-((1R,2S,3R)-1,2,3,4-tetrahydroxybutyl)-1H-imidazole-2-carboxamide (16). To a solution of acid **15** (500 mg, 1.24 mmol) in DCM (4 mL) was added HATU (520 mg, 1.37 mmol), dimethylamine hydrochloride (202 mg, 2.48 mmol), and triethylamine (517 μL, 3.72 mmol). After 20 h, the reaction was treated with an additional portion of HATU (520 mg, 1.37 mmol) and dimethylamine hydrochloride (202 mg, 2.48 mmol). After another 18 h, the reaction was concentrated and purified by flash chroma-

tography (20–40% EtOAc:hexane eluent) to give a oil, which was dissolved in ethanol (8 mL). The solution was sparged with nitrogen for 10 min before the addition of palladium hydroxide on carbon (10 wt %, 100 mg). The reaction vessel was charged with H₂ (65 psi) and stirred vigorously for 20 h. At completion, the reaction was filtered, and the filtrate evaporated to provide an oil, which was dissolved in acetone and cooled to 0 °C in an ice bath. The solution was treated with 2:1 conc HCl:water (6 mL) and the reaction was allowed to warm to room temperature. After 18 h, the reaction was concentrated to provide **16** (23 mg, 7% yield, 2 steps) as a white solid. ¹H NMR (400 MHz, MeOD) δ ppm 7.54 (s, 1 H), 5.20 (s, 1 H), 3.75–3.86 (m, 2 H), 3.63–3.73 (m, 2 H), 3.16 (s, 6 H). ¹³C NMR (100 MHz, 1.0 M DCl in D₂O) δ ppm 156.09, 136.47, 135.67, 117.52, 72.79, 70.77, 64.59, 62.98, 38.58, 36.09. MS (EI) *m/z*: 260 [M + H]⁺. HRMS calcd for C₁₀H₁₇N₃O₅ [M + H]⁺ 260.1246, found 260.1231. HPLC (C30 Develosil RP Aqueous 4.6 mm × 50 mm, 5–80% [methanol/water/TFA (95/5/0.1)]:water with 0.1% TFA, 4 min gradient) *t*_R = 0.35 min, 100% integrated area.

(1R,2S,3R)-1-(2-(1,1-Difluoroethyl)-1H-imidazol-4-yl)butane-1,2,3,4-tetraol (17). THI-bisketal (see preparation of **9**) (2.0 g, 6.45 mmol) was dissolved in DCM (20 mL) and cooled to 0 °C in an ice bath. A solution of diethylaminosulfur trifluoride (3.12 g, 19.35 mmol) in DCM (10 mL) was added in dropwise via syringe to the cooled solution. Then the reaction was allowed to warm to room temperature and maintained for 3 h and then cooled to 0 °C before quenching by slow addition of sat. aq NaHCO₃ (20 mL). The ice bath was removed, and the reaction mixture was stirred at room temperature for 10 min and then transferred to a separatory funnel. The layers were separated, and the aqueous layer was washed with DCM (10 mL). The combined organics were concentrated, and the resulting crude material was purified by preparatory HPLC. The resulting intermediate was lyophilized to provide a white solid, which was dissolved in THF (10 mL) and treated with 1 N aq HCl (10 mL). The reaction was then heated to 50 °C for 3 h. At completion, the reaction was concentrated and then redissolved in water (40 mL) and lyophilized to provide **17** (0.84 g, 53% yield, 2 steps) as a white powder. ¹H NMR (400 MHz, MeOD) δ ppm 7.57 (s, 1 H), 5.19 (d, *J* = 1.3 Hz, 1 H), 3.73–3.85 (m, 2 H), 3.61–3.73 (m, 2 H), 2.20 (t, *J* = 13.2 Hz, 3 H). ¹⁹F NMR (376 MHz, MeOD) δ ppm –91.65, –88.21. MS (EI) *m/z*: 253 [M + H]⁺. HRMS calcd for C₉H₁₄F₂N₂O₄ [M + H]⁺ 253.1000, found 253.0988. HPLC (Sunfire C18 4.6 mm × 50 mm, 0% MeCN:10 mM aq NH₄OAc, 4 min isocratic) *t*_R = 3.10 min, 98% integrated area.

(1R,2S,3R)-1-(2-(Perfluoroethyl)-1H-imidazol-4-yl)butane-1,2,3,4-tetraol (20). To a solution of benzyl 2,2,3,3,3-pentafluoropropionate³⁴ (0.253 g, 1.00 mmol) in methanol (2.0 mL) was added fructosamine-HOAc **18** (0.24 g, 1.00 mmol). The reaction was maintained at room temperature overnight. The reaction was then treated with a 25 wt % solution of sodium methoxide (0.06 g, 1.10 mmol) in MeOH. The reaction was stirred at room temperature for 4 h before the reaction was adjusted to pH ~4 with acetic acid. The reaction was diluted with water (3 mL) and purified directly by HPLC. The product was lyophilized to provide **20** (6 mg, 2%) as a white powder. ¹H NMR (400 MHz, MeOD) δ ppm 7.16 (s, 1 H) 4.94 (d, *J* = 1.8 Hz, 1 H) 3.71 (dd, *J* = 11.1, 3.0 Hz, 1 H) 3.58–3.67 (m, 2 H) 3.54 (dd, *J* = 10.9, 5.1 Hz, 1 H). MS (EI) *m/z*: 307 [M + H]⁺. HRMS calcd for C₉H₁₁F₅N₂O₄ [M + H]⁺ 307.0717, found 307.0708. HPLC (Sunfire C18 4.6 mm × 50 mm, 5–50% MeCN:10 mM aq NH₄OAc, 6 min gradient) *t*_R = 3.13 min, 100% integrated area.

Phenyl(4-((1R,2S,3R)-1,2,3,4-tetrahydroxybutyl)-1H-imidazol-2-yl)methanone (21). Prepared according to the general procedure B from fructosamine-HOAc **18** (0.782 g, 3.27 mmol) and 2,2-difluoro-2-phenylacetone nitrile (500 mg, 3.27 mmol) to provide the spontaneous hydrolysis product, ketone **21** (350 mg, 34% yield) as a yellow solid. ¹H NMR (400 MHz, 1.0 M DCl in D₂O) δ ppm 8.03 (d, *J* = 7.3 Hz, 1 H) 7.68 (t, *J* = 7.5 Hz, 1 H) 7.54 (t, *J* = 7.8 Hz, 1 H) 7.43 (s, 1 H) 5.02 (d, *J* = 3.3 Hz, 1 H) 3.82 (td, *J* = 7.8, 3.0 Hz, 1 H) 3.70–3.78 (m, 1 H) 3.60 (dd, *J* = 11.5, 6.3 Hz, 1 H). ¹³C NMR (100 MHz, 1.0 M DCl in D₂O) δ ppm 180.45, 139.24, 138.53,

135.84, 134.08, 130.18, 129.67, 119.88, 73.11, 70.99, 65.16, 63.22. MS (EI) m/z : 293 [M + H]⁺. HRMS calcd for C₁₄H₁₆N₂O₅ [M + H]⁺ 293.1137, found 293.1162. HPLC (Sunfire C18 4.6 mm × 50 mm, 5–90% MeCN:10 mM aq NH₄OAc, 3 min gradient) t_R = 0.80 min, 100% integrated area.

(1R,2S,3R)-1-(2-(2-Methylthiazol-4-yl)-1H-imidazol-4-yl)butane-1,2,3,4-tetraol (22). Prepared according to the general procedure B from fructosamine-HOAc **18** (1.00 g, 4.13 mmol) and 2-methylthiazole-4-carbonitrile (0.50 g, 4.13 mmol) to provide **22** (0.68 g, 58% yield). ¹H NMR (400 MHz, MeOD) δ ppm 7.40 (s, 1 H) 7.32 (d, J = 3.3 Hz, 1 H) 6.39 (dd, J = 3.6, 0.9 Hz, 1 H) 3.76–3.89 (m, 2 H) 3.67–3.75 (m, 2 H) 2.46 (s, 3 H). ¹³C NMR (100 MHz, 1.0 M DCl in D₂O) δ ppm 171.51, 138.56, 136.39, 134.69, 116.74, 108.40, 72.85, 70.85, 64.68, 62.98, 18.16. MS (EI) m/z : 286 [M + H]⁺. HRMS calcd for C₁₁H₁₅N₃O₄S [M + H]⁺ 286.0862, found 286.0842. HPLC (Zorbax C8 4.6 mm × 150 mm, 5–90% MeCN:10 mM aq NH₄OAc, 3 min gradient) t_R = 1.76 min, 99% integrated area.

(1R,2S,3R)-1-(2-(5-methylthiazol-4-yl)-1H-imidazol-4-yl)butane-1,2,3,4-tetraol (23). Prepared according to the General procedure B from fructosamine-HOAc **18** (2.00 g, 8.25 mmol) and 5-methylthiazole-4-carbonitrile³⁵ (1.02 g, 8.25 mmol) to provide **23** (1.70 g, 72% yield). ¹H NMR (400 MHz, MeOD) δ ppm 9.01 (s, 1 H) 7.55 (s, 1 H) 5.24 (d, J = 1.3 Hz, 1 H) 3.78–3.89 (m, 2 H) 3.67–3.77 (m, 2 H) 2.77 (s, 3 H). ¹³C NMR (100 MHz, 1.0 M DCl in D₂O) δ ppm 155.22, 140.38, 137.84, 134.89, 133.71, 117.14, 72.84, 70.84, 64.63, 62.98, 11.52. MS (EI) m/z : 286 [M + H]⁺. HRMS calcd for C₁₁H₁₅N₃O₄S [M + H]⁺ 286.0862, found 286.0864. HPLC (Luna Phenyl-hexyl 4.6 mm × 50 mm, 5–90% MeCN:10 mM aq NH₄OAc, 3 min gradient) t_R = 0.93 min, 100% integrated area.

(1R,2S,3R)-1-(2-(Thiazol-4-yl)-1H-imidazol-4-yl)butane-1,2,3,4-tetraol (24). Prepared according to the general procedure B from fructosamine-HOAc **18** (0.93 g, 3.88 mmol) and 5-methylthiazole-4-carbonitrile (0.43 g, 3.88 mmol) to provide **24** (95 mg, 9% yield). ¹H NMR (400 MHz, 1.0 M DCl in D₂O) δ ppm 9.01 (d, J = 1.8 Hz, 1 H), 7.94 (d, J = 1.8 Hz, 1 H), 7.19 (s, 1 H), 4.95 (d, J = 3.8 Hz, 1 H), 3.84 (dd, J = 7.0, 3.8 Hz, 1 H), 3.67–3.80 (m, 2 H), 3.59 (dd, J = 11.5, 6.5 Hz, 1 H). ¹³C NMR (100 MHz, 1.0 M DCl in D₂O) δ ppm 157.72, 139.06, 138.58, 134.67, 123.70, 116.73, 72.85, 70.85, 64.69, 62.98. MS (EI) m/z : 272 [M + H]⁺. HRMS calcd for C₁₀H₁₃N₃O₄S [M + H]⁺ 271.0627, found 272.0693. HPLC (HILIC Silica 4.6 mm × 50 mm, 97–40% MeCN:10 mM aq NH₄OAc, 3 min gradient) t_R = 1.21, 100% integrated area.

(1R,2S,3R)-1-(2-(Oxazol-4-yl)-1H-imidazol-4-yl)butane-1,2,3,4-tetraol (25). Prepared according to the general procedure B from fructosamine-HOAc **18** (510 mg, 2.13 mmol) and oxazole-4-carbonitrile (200 mg, 2.13 mmol) to provide **25** (64 mg, 12% yield). ¹H NMR (400 MHz, MeOD) δ ppm 8.29 (s, 1 H), 8.22 (s, 1 H), 7.12 (br s, 1 H), 5.01 (br s, 1 H), 3.71–3.88 (m, 3 H), 3.56–3.71 (m, 1 H). ¹³C NMR (100 MHz, 1.0 M DCl in D₂O) δ ppm 154.05, 140.93, 136.68, 134.86, 125.27, 116.84, 72.85, 70.83, 64.66, 62.98. MS (EI) m/z : 256 [M + H]⁺. HRMS calcd for C₁₀H₁₃N₃O₅ [M + H]⁺ 256.0933, found 256.0936. HPLC (Sunfire C18 4.6 mm × 50 mm, 10–90% MeCN:10 mM aq NH₄OAc, 2 min gradient) t_R = 0.30 min, 100% integrated area.

(1R,2S,3R)-1-(2-(1-Benzyl-1H-1,2,4-triazol-3-yl)-1H-imidazol-4-yl)butane-1,2,3,4-tetraol (26). Prepared according to the general procedure B from fructosamine-HOAc (2.73 g, 11.40 mmol) and 1-benzyl-1H-1,2,4-triazole-3-carbonitrile³⁶ (2.1 g, 11.40 mmol) to provide **26** (3.21 g, 81% yield). ¹H NMR (400 MHz, MeOD) δ ppm 8.80 (s, 1 H), 7.51 (s, 1 H), 7.33–7.45 (m, 5 H), 5.58 (s, 2 H), 5.21 (d, J = 1.3 Hz, 1 H), 3.76–3.86 (m, 2 H), 3.66–3.73 (m, 2 H). MS (EI) m/z : 346 [M + H]⁺. HRMS calcd for C₁₆H₂₀N₅O₄ [M + H]⁺ 346.1515, found 346.1501. HPLC (Sunfire C18 4.6 mm × 50 mm, 5–90% [methanol/water/TFA (95/5/0.1)]:water with 0.1% TFA, 3 min gradient) t_R = 1.89 min, 99% integrated area.

General Procedure D: (1R,2S,3R)-1-(2-(1H-1,2,4-Triazol-3-yl)-1H-imidazol-4-yl)butane-1,2,3,4-tetraol (27). A solution of **26** (275 mg, 0.80 mmol) in methanol (10 mL) and 0.5 M aqueous HCl (14 mL) was sparged with nitrogen for 10 min. Then, palladium hydroxide on carbon (20% w/w, 100 mg) was added, and the reaction vessel was charged with H₂ (65 psi). After 18 h, the reaction was sparged with nitrogen and then filtered over a pad of celite and washed with methanol (10 mL). The solvent was removed to give an off white solid which was then triturated with ether:THF (1:1) to give the deprotected triazole **27** (180 mg, 100% yield) as an off white solid. ¹H NMR (400 MHz, MeOD) δ ppm 8.72 (s, 1 H), 7.54 (s, 1 H), 5.24 (d, J = 1.3 Hz, 1 H), 3.78–3.88 (m, 2 H), 3.66–3.76 (m, 2 H). ¹³C NMR (100 MHz, 1.0 M DCl in D₂O) δ ppm 148.04, 145.55, 135.49, 135.09, 117.08, 72.39, 70.40, 64.25, 62.57. MS (EI) m/z : 256 [M + H]⁺. HRMS calcd for C₁₆H₂₀N₅O₄ [M + H]⁺ 256.1048, found 256.1033. HPLC (Zorbax C8 4.6 mm × 150 mm, 5–90% MeCN:10 mM aq NH₄OAc, 4 min gradient) t_R = 0.80 min, 99% integrated area.

(1R,2S,3R)-1-(1H,1'H-2,2'-biimidazol-4-yl)butane-1,2,3,4-tetraol (28). Prepared according to the general procedure B from fructosamine-HOAc **18** (1.94 g, 8.37 mmol) and 1-benzyl-1H-imidazole-2-carbonitrile (0.78 g, 8.37 mmol) to provide, after hydrogenation by general procedure D, compound **28** (60 mg, 3% yield) as a white solid. ¹H NMR (400 MHz, MeOD) δ ppm 7.14 (d, J = 4.3 Hz, 3 H), 5.02 (s, 1 H), 3.73–3.89 (m, 3 H), 3.66 (br s, 1 H). ¹³C NMR (100 MHz, 1.0 M DCl in D₂O) δ ppm 138.20, 127.82, 122.98, 119.80, 72.87, 70.78, 64.77, 63.02. MS (EI) m/z : 255 [M + H]⁺. HRMS calcd for C₁₀H₁₅N₄O₄ [M + H]⁺ 255.1092, found 255.1085. HPLC (HILIC Silica 4.6 mm × 50 mm, 100–80% MeCN:10 mM aq NH₄OAc, 3 min gradient) t_R = 2.23 min, 99% integrated area.

(1R,2S,3R)-1-(2-(pyrimidin-2-yl)-1H-imidazol-4-yl)butane-1,2,3,4-tetraol (29). Prepared according to the general procedure B from fructosamine-HOAc **18** (2.39 g, 10.00 mmol) and pyrimidine-2-carbonitrile (1.05 g, 10.00 mmol) to provide **29** (0.68 g, 26% yield). ¹H NMR (400 MHz, DMSO-*d*₆) δ ppm 8.82 (d, J = 4.8 Hz, 2 H), 7.39 (t, J = 4.9 Hz, 1 H), 7.14 (s, 1 H), 4.80 (d, J = 1.5 Hz, 1 H), 3.61 (dd, J = 10.7, 3.1 Hz, 2 H), 3.40 (dd, J = 10.8, 5.8 Hz, 2 H). ¹³C NMR (100 MHz, 1.0 M DCl in D₂O) δ ppm 158.25, 151.04, 140.91, 136.18, 122.70, 118.04, 72.43, 70.45, 64.41, 62.62. MS (EI) m/z : 267 [M + H]⁺. HRMS calcd for C₁₁H₁₄N₄O₄ [M + H]⁺ 267.1093, found 267.1079. HPLC (Zorbax C8 4.6 mm × 150 mm, 5% MeCN:10 mM aq NH₄OAc, 4 min isocratic) t_R = 1.01 min, 100% integrated area.

(1R,2S,3R)-1-(2-(Pyrazin-2-yl)-1H-imidazol-4-yl)butane-1,2,3,4-tetraol (30). Prepared according to the general procedure B from fructosamine-HOAc **18** (1.62 g, 7.00 mmol) and pyrazine-2-carbonitrile (0.74 g, 7.00 mmol) to provide **30** (0.72 g, 39% yield). ¹H NMR (300 MHz, deuterium oxide) δ ppm 8.96 (d, J = 1.5 Hz, 1 H), 8.52 (dd, J = 2.7, 1.5 Hz, 1 H), 8.42 (d, J = 2.7 Hz, 1 H), 7.22 (br s, 1 H), 4.91 (br s, 1 H), 3.78 (dd, J = 7.1, 3.6 Hz, 1 H), 3.59–3.75 (m, 2 H), 3.47–3.58 (m, 1 H). ¹³C NMR (100 MHz, 1.0 M DCl in D₂O) δ ppm 146.28, 145.98, 141.42, 140.38, 138.82, 136.66, 118.52, 72.84, 70.85, 64.82, 63.02. MS (EI) m/z : 267 [M + H]⁺. HRMS calcd for C₁₁H₁₄N₄O₄ [M + H]⁺ 267.1093, found 267.1091. HPLC (HILIC Silica 4.6 mm × 50 mm, 100–40% MeCN:10 mM aq NH₄OAc, 3 min gradient) t_R = 1.47 min, 99% integrated area.

(1R,2S,3R)-1-(2-(1,2,4-Oxadiazol-3-yl)-1H-imidazol-4-yl)butane-1,2,3,4-tetraol (31). Prepared according to the general procedure B from fructosamine-HOAc **18** (478 mg, 2.00 mmol) and 1,2,4-oxadiazole-3-carbonitrile (512 mg, 2.00 mmol) to provide **31** (205 mg, 40% yield). ¹H NMR (400 MHz, 1.0 M DCl in D₂O) δ ppm 9.43 (s, 1 H), 7.64 (s, 1 H), 5.24 (s, 1 H), 3.72–3.84 (m, 3 H), 3.61–3.68 (m, J = 13.1, 6.8 Hz, 1 H). ¹³C NMR (100 MHz, 1.0 M DCl in D₂O) δ ppm 169.3, 157.4, 138.6, 132.8, 119.9, 73.8, 71.6, 65.8, 63.8. MS (EI) m/z : 257 [M + H]⁺. HRMS calcd for C₉H₁₂N₄O₅ [M + H]⁺ 257.0886, found 257.0870. HPLC (Luna Phenyl-hexyl 4.6 mm × 50 mm, 5% [methanol/water/TFA (95/5/0.1)]:water, isocratic) t_R = 2.41 min, 100% integrated area.

(1R,2S,3R)-1-(1'-Methyl-1H,1'H-2,4'-biimidazol-4-yl)butane-1,2,3,4-tetraol (32). Prepared according to the general procedure B from fructosamine-HOAc **18** (2.00 g, 8.25 mmol) and 1-methyl-1H-imidazole-4-carbonitrile (0.88 g, 8.25 mmol) to provide **32** (0.90 g, 41% yield). ¹H NMR (400 MHz, MeOD) δ ppm 9.22 (s, 1 H), 8.33 (d, *J* = 1.5 Hz, 1 H), 7.65 (s, 1 H), 5.26 (d, *J* = 1.3 Hz, 1 H), 4.10 (s, 3 H), 3.78–3.88 (m, 2 H), 3.68–3.77 (m, 2 H). ¹³C NMR (100 MHz, 1.0 M DCl in D₂O) δ ppm 138.59, 136.30, 132.08, 125.65, 118.05, 117.42, 72.93, 70.83, 64.67, 63.06, 36.77. MS (EI) *m/z*: 269 [M + H]⁺. HRMS calcd for C₁₁H₁₆N₄O₄ [M + H]⁺ 269.1250, found 261.1242. HPLC (Zorbax C8 4.6 mm × 150 mm, 5–90% [methanol/water/TFA (95/5/0.1)]:water, 3 min gradient) *t*_R = 0.32 min, 100% integrated area.

1-(4-((1R,2R,3R)-1,2,3,4-Tetrahydroxybutyl)-1H-imidazol-2-yl)ethanone (33). The Amadori and Büchi rearrangements detailed in general procedure A and general procedure B, respectively, were applied to D-galactose (5.00 g, 27.78 mmol) to generate **33** (60 mg, 1% yield, 2 steps). ¹H NMR (400 MHz, 1.0 M DCl in D₂O) δ ppm 7.24 (s, 1 H), 4.67 (br s, 1 H), 3.80–3.88 (m, 1 H), 3.76 (dd, *J* = 8.1, 2.5 Hz, 1 H), 3.49–3.60 (m, 2 H), 2.44 (m, 2 H), 2.44 (s, 3 H). MS (EI) *m/z*: 231 [M + H]⁺. HRMS calcd for C₉H₁₅N₂O₅ [M + H]⁺ 231.0981, found 231.0968. HPLC (Sunfire C18 4.6 mm × 50 mm, 10–90% MeCN:10 mM aq NH₄OAc, 2 min gradient) *t*_R = 0.22 min, 100% integrated area.

1-(4-((1S,2R,3S)-1,2,3,4-Tetrahydroxybutyl)-1H-imidazol-2-yl)ethanone (34). The Amadori and Büchi rearrangements detailed in general procedure A and general procedure B, respectively, were applied to L-(–)-glucose (5.00 g, 27.78 mmol) to generate **34** (2.76 g, 44% yield, 2 steps). ¹H NMR (300 MHz, 1.0 M DCl in D₂O) δ ppm 7.25 (s, 1 H), 4.86 (d, *J* = 1.7 Hz, 1 H), 3.32–3.48 (m, 3 H), 3.23–3.32 (m, 1 H), 2.31 (s, 3 H). MS (EI) *m/z*: 231 [M + H]⁺. HRMS calcd for C₉H₁₅N₂O₅ [M + H]⁺ 231.0981, found 231.0970. HPLC (C30 Develosil RP Aqueous 4.6 mm × 50 mm, 2–40% [methanol/water/TFA (95/5/0.1)]:water with 0.1% TFA, 5 min gradient) *t*_R = 2.14 min, 100% integrated area.

1-(4-((1R,2R,3R)-2,3,4-Trihydroxy-1-methoxybutyl)-1H-imidazol-2-yl)ethanone (36). The Amadori and Büchi rearrangements detailed in general procedure A and general procedure B, respectively, were applied to D-(+)-glucose-3-hydroxymethyl ether **35** (1.90 g, 9.60 mmol) to generate **36** (22 mg, 1.0% yield) after HPLC purification. ¹H NMR (400 MHz, MeOD) δ ppm 7.30 (s, 1 H), 4.65 (d, *J* = 3.0 Hz, 1 H), 3.79 (dd, *J* = 11.0, 3.0 Hz, 1 H), 3.70–3.76 (m, 1 H), 3.59–3.68 (m, 2 H), 3.35 (d, *J* = 8.0 Hz, 3 H), 1.92 (s, 3 H). MS (EI) *m/z*: 245 [M + H]⁺. HRMS calcd for C₁₀H₁₇N₂O₅ [M + H]⁺ 245.1137, found 245.1115. HPLC (Sunfire C18 4.6 mm × 50 mm, 6–30% [methanol/water/TFA (95/5/0.1)]:water with 0.1% TFA, 5 min gradient) *t*_R = 1.07 min, 100% integrated area.

(2S,3S,4R)-4-(2-Acetyl-1H-imidazol-4-yl)-2,3,4-trihydroxy-N,N-dimethylbutanamide (38). The Amadori and Büchi rearrangements detailed in general procedure A and general procedure B, respectively, were applied to D-(+)-glucose-6-dimethylamide **37** (2.12 g, 9.60 mmol) to generate **38** (60 mg, 2.0% yield) after purification by preparatory HPLC. ¹H NMR (400 MHz, 1.0 M DCl in D₂O) δ ppm 7.31 (s, 1 H), 5.00 (d, *J* = 3.3 Hz, 1 H), 4.75 (d, *J* = 7.8 Hz, 1 H), 3.95 (dd, *J* = 7.8, 3.3 Hz, 1 H), 3.07 (s, 3 H), 2.84 (s, 3 H), 2.53 (s, 3 H). MS (EI) *m/z*: 272 [M + H]⁺. HRMS calcd for C₁₁H₁₇N₃O₅ [M + H]⁺ 272.1246, found 272.1200. HPLC (Sunfire C18 4.6 mm × 50 mm, 10–90% [methanol/water/TFA (95/5/0.1)]:water, 4 min gradient) *t*_R = 0.37 min, 96% integrated area.

Acknowledgment. We thank the analytical group at Lexicon Pharmaceuticals in Princeton, NJ, for their assistance in the characterization of compounds and the animal handling and vivarium operation groups in The Woodlands, TX for their maintenance of animal resources.

Note Added after ASAP Publication. This manuscript was released ASAP on May 21, 2009, with an incomplete author listing. The correct version was posted on July 2, 2009.

Supporting Information Available: HPLC conditions for determining purity of all final products, select elemental analyses, and characterization data of final products. This material is available free of charge via the Internet at <http://pubs.acs.org>.

References

- (1) (a) Kitatani, K.; Idkowiak-Baldys, J.; Hannun, Y. A. The sphingolipid salvage pathway in ceramide metabolism and signaling. *Cell. Signaling* **2008**, *20*, 1010–1018. (b) Gomez-Munoz, A.; Steinbrecher, U. P. Control of cell signaling by ceramides, sphingosine-1-phosphate and ceramide-1-phosphate. *Recent Res. Dev. Lipids* **2004**, *7*, 65–86. (c) Smith, W. L.; Merrill, A. H. Sphingolipid metabolism and signaling. *J. Biol. Chem.* **2002**, *277*, 25841–25842. (d) Lahiri, S.; Futerman, A. H. The metabolism and function of sphingolipids and glycosphingolipids. *Cell. Mol. Life Sci.* **2007**, *64*, 2270–2284.
- (2) (a) Rivera, J.; Proia, R. L.; Olivera, A. The alliance of sphingosine-1-phosphate and its receptors in immunity. *Nat. Rev.* **2008**, *8*, 753–763. (b) Gomez-Munoz, A.; Steinbrecher, U. P. Control of cell signaling by ceramides, sphingosine-1-phosphate and ceramide-1-phosphate. *Recent Res. Dev. Lipids* **2004**, *7*, 65–86.
- (3) (a) Reiss, U.; Oskoui, B.; Zhou, J.; Gupta, V.; Sooriyakumaran, P.; Kelly, S.; Wang, E.; Merrill, A. H.; Saba, J. J. Sphingosine-phosphate lyase enhances stress-induced ceramide generation apoptosis. *J. Biol. Chem.* **2004**, *279*, 1281–1290. (b) Moore, A. N.; Kampfl, A. W.; Zhao, X.; Hayes, R. L.; Dask, P. K. Sphingosine 1-phosphate induces apoptosis of cultured hippocampal neurons that requires protein phosphatases and activator protein-1 complexes. *Neuroscience* **1999**, *94*, 405–415.
- (4) (a) Hait, N. C.; Oskeritizian, C. A.; Paugh, S. W.; Milstein, S.; Spiegel, S. Sphingosine kinases, sphingosine 1-phosphate, apoptosis and disease. *Biochim. Biophys. Acta* **2006**, *1758*, 2016–2026. (b) Saba, J. D.; Hla, T. Point-counterpoint of sphingosine 1-phosphate metabolism. *Circ. Res.* **2004**, *94*, 724–734. (c) Pyne, S.; Pyne, N. J. Sphingosine 1-phosphate signaling in mammalian cells. *Biochem. J.* **2000**, *349*, 385–402.
- (5) (a) Wang, W.; Huang, M.-C.; Goetzl, E. J. Type 1 sphingosine 1-phosphate G protein-coupled receptor (S1P1) mediation of enhanced IL-4 generation by CD4 T cells from S1P1 transgenic mice. *J. Immunol.* **2007**, *178*, 4885–4890. (b) Chi, H.; Flavell, R. A. Cutting edge: regulation of T cell trafficking and primary immune responses by sphingosine 1-phosphate receptor 1. *J. Immunol.* **2005**, *174*, 2485–2488. (c) Goetzl, E. J.; Liao, J.-J.; Huang, M.-C. Regulation of the roles of sphingosine 1-phosphate and its type 1 G protein-coupled receptor in T cell immunity and autoimmunity. *Mol. Cell Biol. Lipids* **2008**, *1781*, 503–507.
- (6) For a general review, see: (a) Goetzl, E. J.; Wang, W.; McGiffert, C.; Huang, M.-C.; Graeler, M. H. Sphingosine 1-phosphate and its G protein-coupled receptors constitute a multifunctional immunoregulatory system. *J. Cell. Biochem.* **2004**, *92*, 1104–1114.
- (7) Yoshikawa, M.; Yokokawa, Y.; Okuno, Y.; Yagi, N.; Murakami, N. Synthesis, Immunosuppressive Activity, and Structure-Activity Relationships of Myriocin Analogs, 2-*epi*-Myriocin, 14-Deoxymyriocin, Z-14-Deoxymyriocin, and Nor-deoxymyriocin. *Chem. Pharm. Bull.* **1995**, *43*, 1647–1653.
- (8) (a) Miyake, Y.; Kozutsumi, Y.; Nakamura, S.; Fujita, T.; Kawasaki, T. Serine palmitoyltransferase is the primary target of a sphingosine-like immunosuppressant, ISP-1/ myriocin. *Biochem. Biophys. Res. Commun.* **1995**, *211*, 396–403. (b) Chen, J. K.; Lane, W. S.; Schreiber, S. L. The Identification of Myriocin-Binding proteins. *Chem. Biol.* **1999**, *6*, 221–235.
- (9) (a) Yoshikawa, M.; Yokokawa, Y.; Okuno, Y.; Yagi, N.; Murakami, N. Syntheses, immunosuppressive activity, and structure-activity relationships of myriocin analogs, 2-*epi*-myriocin 14-deoxomyriocin, Z-14-deoxomyriocin, and nor-deoxomyriocins. *Chem. Pharm. Bull.* **1995**, *43*, 1647–1653. (b) Fujita, T.; Hirose, R.; Hamamichi, N.; Kitao, Y.; Sasaki, S.; Yoneta, M.; Chiba, K. 2-Substituted 2-aminoethanol: minimum essential structure for immunosuppressive activity of ISP-1 (myriocin). *Bioorg. Med. Chem. Lett.* **1995**, *5*, 1857–1860.
- (10) (a) Rivera, J.; Proia, R. L.; Olivera, A. The alliance of sphingosine-1-phosphate and its receptors in immunity. *Nat. Rev. Immunol.* **2008**, *8*, 753–763. (b) Billich, A.; Baumruker, T. Sphingolipid Metabolizing Enzymes as Novel Therapeutic Targets. In *Lipids in Health and Disease*; Quinn, P. J.; Wang, X., Eds.; Springer Science Business Media: New York, 2008; 487–522.
- (11) (a) Igarashi, Y. Functional roles of sphingosine, sphingosine 1-phosphate, and methylsphingosines: in regard to membrane sphingolipid signaling pathways. *J. Biochem.* **1997**, *122*, 1080–1087. (b) Elrick, M. J.; Fluss, S.; Colombini, M. Sphingosine, a product of ceramide hydrolysis, influences the formation of ceramide channels. *Biophys. J.* **2006**, *91*, 1749–1756.
- (12) SK I is believed to play the more dominant role. See: (a) Kharel, Y.; Lee, S.; Snyder, A. H.; Sheasley-O'Neill, S. L.; Morris, M. A.; Setiady,

- Y.; Zhu, R.; Zigler, M. A.; Burcin, T. L.; Ley, K.; Tung, K. S. K.; Engelhard, V. H.; Macdonald, T. L.; Pearson-White, S.; Lynch, K. R. Sphingosine Kinase 2 Is Required for Modulation of Lymphocyte Traffic by FTY720. *J. Biol. Chem.* **2005**, *280*, 36865–36872. (b) Baumruker, T.; Bornancin, F.; Billich, A. The role of sphingosine and ceramide kinases in inflammatory responses. *Immunol. Lett.* **2005**, *96*, 175–185.
- (13) (a) Johnson, K. R.; Johnson, K. Y.; Becker, K. P.; Bielawski, J.; Mao, C.; Obeid, L. M. Role of human sphingosine-1-phosphate phosphatase 1 in the regulation of intra- and extracellular sphingosine-1-phosphate levels and cell viability. *J. Biol. Chem.* **2003**, *278*, 34541–34547. (b) Mechtcheriakova, D.; Wlachos, A.; Sobanov, J.; Kopp, T.; Reuschel, R.; Bornancin, F.; Cai, R.; Zemann, B.; Urtz, N.; Stingl, G.; Zlabinger, G.; Woisetschlaeger, M.; Baumruker, T.; Billich, A. Sphingosine 1-phosphate phosphatase 2 is induced during inflammatory responses. *Cell. Signalling* **2007**, *19*, 748–760.
- (14) (a) Bandhuvula, P.; Fyrst, H.; Saba, J. D. A rapid fluorescence assay for sphingosine-1-phosphate lyase enzyme activity. *J. Lipid Res.* **2007**, *48*, 2769–2778. (b) Bandhuvula, P.; Saba, J. D. Sphingosine-1-phosphate lyase in immunity and cancer: silencing the siren. *Trends Mol. Med.* **2007**, *13*, 210–217.
- (15) Vogel, P.; Donoviel, M. S.; Read, R.; Hansen, G. M.; Hazlewood, J.; Anderson, S.; Sun, W.; Swaffield, J.; Oravec, T. Incomplete Inhibition of Sphingosine 1-Phosphate Lyase Modulates Immune System Function yet Prevents Early Lethality and Non-Lymphoid Lesions. *PLoS One* **2008**, *4*, 4112.
- (16) It has been established that FTY720 is phosphorylated by sphingosine kinases in vivo and that phospho-FTY720 is the active S1P agonist. See: (a) Billich, A.; Bornancin, F.; Devay, P.; Mechtcheriakova, D.; Urtz, N.; Baumruker, T. Phosphorylation of the Immunomodulatory Drug FTY720 by Sphingosine Kinases. *J. Biol. Chem.* **2003**, *278*, 47408–47415. (b) Zemann, B.; Kinzel, B.; Mueller, M.; Reuschel, R.; Mechtcheriakova, D.; Urtz, N.; Bornancin, F.; Baumruker, T.; Billich, A. Sphingosine kinase type 2 is essential for lymphopenia induced by the immunomodulatory drug FTY720. *Blood* **2006**, *107*, 1454–1458.
- (17) Assay conducted with [³³P]-S1P pyridoxal phosphate and a lysate of S1P lyase. Production of [³³P]-phosphoethanolamine was monitored to determine lyase activity.
- (18) FTY720 was used as a positive control in parallel with vehicle control group (*n* = 5 mice/group).
- (19) Kroepfien, U.; Rosdorfer, J.; Van der Greef, J.; Long, R. C., Jr.; Goldstein, J. H. 2-Acetyl-4(5)-(1,2,3,4-tetrahydroxybutyl)imidazole: detection in commercial caramel color III and preparation by a model browning reaction. *J. Org. Chem.* **1985**, *50*, 1131–1133.
- (20) (a) Spector, R.; Huntoon, S. Effects of Caramel Color (Ammonia Process) on Mammalian Vitamin B6 Metabolism. *Toxicol. Appl. Pharmacol.* **1982**, *62*, 172–178. (b) Houben, G. F.; Kuijpers, M. H. M.; Van Loveren, H.; Penninks, A. H.; Sinkeldam, E. J.; Seinen, W. Effects of ammonia caramel and tetrahydroxybutylimidazole on the immune system of rats. *Arch. Toxicol.* **1989**, *13*, 183–187. (c) Gobin, S. J. P.; Phillips, J. A. Immunosuppressive effects of 2-acetyl-4-tetrahydroxybutyl imidazole (THI) in the rat. *Clin. Arch. Toxicol. Exp. Immunol.* **1991**, *85*, 335–340. (d) Bradbury, M. G.; Doherty, K. V.; Parish, C. R.; Lyons, A. B. The immunosuppressive compound 2-acetyl-4-tetrahydroxybutyl imidazole inhibits the allogeneic mixed lymphocyte reaction by sequestration of a recirculating subpopulation of T cells. *Immunology* **1996**, *87*, 80–85. (e) Gugsyan, R.; Coward, A.; O'Connor, L.; Shortman, K.; Scollay, R. Emigration of mature T cells from the thymus is inhibited by the imidazole-based compound 2-acetyl-4-tetrahydroxybutylimidazole. *Immunology* **1998**, *93*, 398–404.
- (21) Schwab, S. R.; Pereira, J. P.; Matloubian, M.; Xu, Y.; Huang, Y.; Cyster, J. G. Lymphocyte Sequestration Through S1P Lyase Inhibition and Disruption of S1P Gradients. *Science* **2005**, *309*, 1735–1739.
- (22) Sanna, M. G.; Liao, Jiayu; Jo, E.; Alfonso, C.; Ahn, M.-Y.; Peterson, M. S.; Webb, B.; Lefebvre, S.; Chun, J.; Gray, N.; Rosen, H. Sphingosine 1-phosphate (S1P) receptor subtypes S1P1 and S1P3, respectively, regulate lymphocyte recirculation and heart rate. *J. Biol. Chem.* **2004**, *279*, 13839–13848.
- (23) (a) Pyne, S. G.; Ung, A. T. Diastereoselective Synthesis of (1S,2S,3R)- and (1R,2R,3R)-2-Acetyl-5-(1,2,3,4-tetrahydroxybutyl)thiazole. *Synlett* **1998**, *3*, 280–282. (b) Ung, A. T.; Pyne, S. G.; Skelton, B. W.; White, A. H. Asymmetric synthesis of (1R,2S,3R)-2-acetyl-5-(1,2,3,4-tetrahydroxybutyl)thiazole. *Tetrahedron* **1996**, *52*, 14069–14078.
- (24) (a) Hodge, John, E.; Rist, Carl, E. Amadori rearrangement under new conditions and its significance for nonenzymatic browning reactions. *J. Am. Chem. Soc.* **1953**, *75*, 316–322. (b) Hodge, J. E.; Fisher, B. E. Amadori Rearrangement Products. In *Methods in Carbohydrate Chemistry, Volume II: Reactions of Carbohydrates* Whistler, R. L., Wolfrom, M. L., Bemiller, J. N., Eds.; Academic Press: New York, 1963; Vol. II, pp 99–103.
- (25) Buchi, G.; Halweg, K. M. A Convenient Synthesis of 2-Acetyl-4(5)-(1(R),2(S),3(R),4-tetrahydroxybutyl)-imidazole. *J. Am. Chem. Soc.* **1984**, *50*, 1134–1136.
- (26) Murata, N.; Sato, K.; Kon, J.; Tomura, H.; Okajima, F. Quantitative Measurement of Sphingosine-1-Phosphate by Radioreceptor-Binding Assay. *Anal. Biochem.* **2000**, *282*, 115–120.
- (27) Mukhopadhyay, D.; Howell, K. S.; Riezman, H.; Capitani, G. *J. Biol. Chem.* **2008**, *283*, 20159–20169.
- (28) (a) Drews, J. Drug Discovery: A Historical Perspective. *Science* **2000**, *287*, 1960–1964. (b) Sams-Dodd, F. Target-based drug discovery: is something wrong? *Drug Discovery Today* **2005**, *10*, 139–147. (c) Sams-Dodd, F. Drug discovery: selecting the optimal approach. *Drug Discovery Today* **2006**, *11*, 465–472.
- (29) Kondoh, M.; Yagi, K. Progress in absorption enhancers based on tight junction. *Expert Opin. Drug Delivery* **2007**, *4*, 275–286.
- (30) To our knowledge, acid catalyzed hydrolysis of α -polyfluorinated imidazoles has not previously been reported. For references involving alkaline catalysis, see: (a) Fujii, S.; Maki, Y.; Kimoto, H.; Cohen, L. A. Synthesis and alkaline hydrolysis of (pentafluoroethyl)imidazoles. *J. Fluorine Chem.* **1987**, *35*, 437–454. (b) Hayahawa, Y.; Kimoto, H.; Cohen, L. A.; Kirk, K. L. Synthesis of (Trifluoromethyl)imidazoles with Additional Electronegative Substituents. An Approach to Receptor-Activated Affinity Labels. *J. Org. Chem.* **1998**, *63*, 9448–9454.
- (31) (a) MSDS for hydrogen fluoride. (b) For a discussion on the effects of HF poisoning, see: Heard, K.; Delgado, J. Oral Decontamination with Calcium or Magnesium Salts Does Not Improve Survival Following Hydrofluoric Acid Ingestion. *J. Toxicol. Clin. Toxicol.* **2003**, *41*, 789–792.
- (32) Hodge, J. E.; Fisher, B. E. Amadori Rearrangement Products. In *Methods in Carbohydrate Chemistry, Volume II: Reactions of Carbohydrates* Whistler, R. L., Wolfrom, M. L., Bemiller, J. N., Eds.; Academic Press: New York, 1963; Vol. II, pp 99–103.
- (33) Hatanaka, M.; Takahashi, K.; Nakamura, S.; Mashino, T. Preparation and antioxidant activity of α -pyridoin and its derivatives. *Bioorg. Med. Chem. Lett.* **2005**, *13*, 6763–6770.
- (34) Nakajima, N.; Saito, M.; Ubukata, M. Preparation and reaction of 4-methoxybenzyl (MPM) and 3,4-dimethoxybenzyl (DMPM) perfluoroimidates. *Tetrahedron Lett.* **1998**, *39*, 5565–5568.
- (35) Abarbri, M.; Thibonnet, J.; Berillon, L.; Dehmel, F.; Rottlander, M.; Knochel, P. Preparation of New Polyfunctional Magnesiumated Heterocycles Using a Chlorine-, Bromine-, or Iodine-Magnesium Exchange. *J. Org. Chem.* **2000**, *65*, 4618–4634.
- (36) Ohta, S.; Kawasaki, I.; Fukuno, A.; Yamashita, M.; Tada, T.; Kawabata, T. Synthesis and application of triazole derivatives. Synthesis of 3- and 5-acyl-1,2,4-triazoles via lithiation of 1-alkyl-1H-1,2,4-triazoles. *Chem. Pharm. Bull.* **1993**, *41*, 1226–1231.